











TECH BRIEFS

NATIONAL AERONAUTICS AND SPACE ADMINISTRATION

-  **Technology Focus**
-  **Computers/Electronics**
-  **Software**
-  **Materials**
-  **Mechanics**
-  **Machinery/Automation**
-  **Manufacturing**
-  **Bio-Medical**
-  **Physical Sciences**
-  **Information Sciences**
-  **Books and Reports**

INTRODUCTION

Tech Briefs are short announcements of innovations originating from research and development activities of the National Aeronautics and Space Administration. They emphasize information considered likely to be transferable across industrial, regional, or disciplinary lines and are issued to encourage commercial application.

Availability of NASA Tech Briefs and TSPs

Requests for individual Tech Briefs or for Technical Support Packages (TSPs) announced herein should be addressed to

National Technology Transfer Center

Telephone No. (800) 678-6882 or via World Wide Web at www2.nttc.edu/leads/

Please reference the control numbers appearing at the end of each Tech Brief. Information on NASA's Commercial Technology Team, its documents, and services is also available at the same facility or on the World Wide Web at www.nctn.hq.nasa.gov.

Commercial Technology Offices and Patent Counsels are located at NASA field centers to provide technology-transfer access to industrial users. Inquiries can be made by contacting NASA field centers and program offices listed below.

NASA Field Centers and Program Offices

Ames Research Center

Lisa L. Lockyer
(650) 604-3009
lisa.l.lockyer@nasa.gov

Dryden Flight Research Center

Gregory Poteat
(661) 276-3872
greg.poteat@dfrc.nasa.gov

Goddard Space Flight Center

Nona Cheeks
(301) 286-5810
Nona.K.Cheeks.1@gsfc.nasa.gov

Jet Propulsion Laboratory

Ken Wolfenbarger
(818) 354-3821
james.k.wolfenbarger@jpl.nasa.gov

Johnson Space Center

Charlene E. Gilbert
(281) 483-3809
commercialization@jsc.nasa.gov

Kennedy Space Center

Jim Aliberti
(321) 867-6224
Jim.Aliberti-1@ksc.nasa.gov

Langley Research Center

Jesse Midgett
(757) 864-3936
jesse.c.midgett@nasa.gov

John H. Glenn Research Center at Lewis Field

Larry Viterna
(216) 433-3484
cto@grc.nasa.gov

Marshall Space Flight Center

Vernotto McMillan
(256) 544-2615
vernotto.mcmillan@msfc.nasa.gov

Stennis Space Center

Robert Bruce
(228) 688-1929
robert.c.bruce@nasa.gov

NASA Program Offices

At NASA Headquarters there are seven major program offices that develop and oversee technology projects of potential interest to industry:

Carl Ray

Small Business Innovation Research Program (SBIR) & Small Business Technology Transfer Program (STTR)
(202) 358-4652 or
cray@nasa.gov

Benjamin Neumann

Innovative Technology Transfer Partnerships (Code TD)
(202) 358-2320
benjamin.j.neumann@nasa.gov

John Mankins

Office of Space Flight (Code TD)
(202) 358-4659 or
john.c.mankins@nasa.gov

Terry Hertz

Office of Aero-Space Technology (Code RS)
(202) 358-4636 or
thertz@nasa.gov

Glen Mucklow

Office of Space Sciences (Code SM)
(202) 358-2235 or
gmucklow@nasa.gov

Roger Crouch

Office of Microgravity Science Applications (Code U)
(202) 358-0689 or
rcrouch@nasa.gov

Granville Paules

Office of Mission to Planet Earth (Code Y)
(202) 358-0706 or
gpaules@mtpe.hq.nasa.gov



TECH BRIEFS

NATIONAL AERONAUTICS AND SPACE ADMINISTRATION



5 Technology Focus: Composites/Plastics

- 5 Brazing SiC/SiC Composites to Metals
- 5 Composite-Material Tanks With Chemically Resistant Liners
- 6 Thermally Conductive Metal-Tube/Carbon-Composite Joints
- 7 Improved BN Coatings on SiC Fibers in SiC Matrices



9 Electronics/Computers

- 9 Iterative Demodulation and Decoding of Non-Square QAM
- 10 Measuring Radiation Patterns of Reconfigurable Patch Antennas on Wafers
- 11 Low-Cutoff, High-Pass Digital Filtering of Neural Signals



13 Software

- 13 Further Improvement in 3DGRAPE
- 13 Ground Support Software for Spaceborne Instrumentation
- 13 MER SPICE Interface
- 13 Simulating Operation of a Planetary Rover
- 14 Analyzing Contents of a Computer Cache
- 14 Discrepancy Reporting Management System



15 Mechanics

- 15 Silicone-Rubber Microvalves Actuated by Paraffin



17 Machinery/Automation

- 17 Hydraulic Apparatus for Mechanical Testing of Nuts



19 Manufacturing

- 19 Heat Control via Torque Control in Friction Stir Welding

- 19 Manufacturing High-Quality Carbon Nanotubes at Lower Cost

- 20 Setup for Visual Observation of Carbon-Nanotube Arc Process



21 Bio-Medical

- 21 Solution Preserves Nucleic Acids in Body-Fluid Specimens
- 21 Oligodeoxynucleotide Probes for Detecting intact Cells



23 Physical Sciences

- 23 Microwave-Spectral Signatures Would Reveal Concealed Objects
- 24 Digital Averaging Phasemeter for Heterodyne Interferometry
- 26 Optoelectronic Instrument Monitors pH in a Culture Medium
- 26 Imaging of γ -Irradiated Regions of a Crystal
- 27 Photodiode-Based, Passive Ultraviolet Dosimeters
- 28 Discrete Wavelength-Locked External Cavity Laser



31 Books & Reports

- 31 Flexible Shields for Protecting Spacecraft Against Debris
- 31 Part 2 of a Computational Study of a Drop-Laden Mixing Layer
- 31 Controllable Curved Mirrors Made From Single-Layer EAP Films
- 31 Demonstration of a Pyrotechnic Bolt-Retractor System

This document was prepared under the sponsorship of the National Aeronautics and Space Administration. Neither the United States Government nor any person acting on behalf of the United States Government assumes any liability resulting from the use of the information contained in this document, or warrants that such use will be free from privately owned rights.



Brazing SiC/SiC Composites to Metals

Success depends on suitable process conditions and adequate titanium contents in brazing alloys.

Marshall Space Flight Center, Alabama

Experiments have shown that active brazing alloys (ABAs) can be used to join SiC/SiC composite materials to metals, with bond strengths sufficient for some structural applications. The SiC/SiC composite coupons used in the experiments were made from polymer-based SiC fiber preforms that were chemical-vapor-infiltrated with SiC to form SiC matrices. Some of the metal coupons used in the experiments were made from 304 stainless steel; others were made from oxygen-free, high-conductivity copper.

Three ABAs were chosen for the experiments: two were chosen randomly from among a number of ABAs that were on hand at the time; the third ABA was chosen because its titanium content (1.25 percent) is less than those of the other two ABAs (1.75 and 4.5 percent, respectively) and it was desired to evaluate the effect of reducing the titanium content, as described below. The characteristics of ABAs that are considered to be beneficial for the purpose of joining SiC/SiC to metal include wettability, reactivity, and adhesion to SiC-based ceramics. Prior to further development, it was verified that

the three chosen ABAs have these characteristics.

For each ABA, suitable vacuum brazing process conditions were established empirically by producing a series of (SiC/SiC)/ABA wetting samples. These samples were then sectioned and subjected to scanning electron microscopy (SEM) and energy-dispersive x-ray spectrometry (EDS) for analysis of their microstructures and compositions. Specimens for destructive mechanical tests were fabricated by brazing of lap joints between SiC/SiC coupons 1/8-in. (≈ 3.2 -mm) thick and, variously, stainless steel or copper tabs. The results of destructive mechanical tests and the SEM/EDS analysis were used to guide the development of a viable method of brazing the affected materials.

The 1.75-percent-Ti ABA was found to be well suited for joining the SiC/SiC composite with 304 stainless steel. The (SiC/SiC)/Cu joints made by use of the 1.75- and 4.5-percent-Ti ABAs were found to be stronger than were the (SiC/SiC)/Cu joints made by use of the 1.25-percent-Ti. At the time of reporting the information for this article, it was believed that the 1.25-percent titanium

content was insufficient for reacting with the SiC/SiC composite; however, it was uncertain whether an observed difficulty in producing joints of acceptably high quality was caused at least in part by surface contaminants that could consume what little titanium was available for reacting with SiC.

The strengths of the (SiC/SiC)/stainless-steel joints tested ranged up to a maximum of 24.5 MPa for joints made with the 1.75-percent Ti ABA. The strengths of the (SiC/SiC)/Cu joints tested ranged up to a maximum of 23.1 MPa for joints made with the 4.5-percent Ti ABA. The preliminary data on the (SiC/SiC)/1.75-percent-Ti ABA/stainless-steel and (SiC/SiC)/4.5-percent-Ti ABA/Cu joints show that the characteristics of the joints are highly predictable — a quality that is desirable for optimization of design.

*This work was done by Wayne S. Steffier of Hyper-Therm High-Temperature Composites, Inc., for Marshall Space Flight Center. Further information is contained in a TSP (see page 1).
MFS-31876*

Composite-Material Tanks With Chemically Resistant Liners

Liner materials are chosen for compatibility with reactive and/or unstable fluids.

Marshall Space Flight Center, Alabama

Lightweight composite-material tanks with chemically resistant liners have been developed for storage of chemically reactive and/or unstable fluids — especially hydrogen peroxide. These tanks are similar, in some respects, to the ones described in “Lightweight Composite-Material Tanks for Cryogenic Liquids” (MFS-31379), *NASA Tech Briefs*, Vol. 25, No. 1 (January, 2001), page 58; however, the present tanks are fabricated by a different procedure and they do not incorporate insulation that would be needed to prevent boil-off of cryogenic fluids.

The manufacture of a tank of this type begins with the fabrication of a reusable multisegmented aluminum mandrel in the shape and size of the desired interior volume. One or more segments of the mandrel can be aluminum bosses that will be incorporated into the tank as end fittings.

The mandrel is coated with a mold-release material. The mandrel is then heated to a temperature of about 400 °F (≈ 200 °C) and coated with a thermoplastic liner material to the desired thickness [typically ≈ 15 mils (≈ 0.38 mm)] by thermal spraying. In the ther-

mal-spraying process, the liner material in powder form is sprayed and heated to the melting temperature by a propane torch and the molten particles land on the mandrel.

The sprayed liner and mandrel are allowed to cool, then the outer surface of the liner is chemically and/or mechanically etched to enhance bonding of a composite overwrap. The etched liner is wrapped with multiple layers of an epoxy resin reinforced with graphite fibers; the wrapping can be done either by manual application of epoxy-impregnated graphite cloth or by winding of

epoxy-impregnated filaments. The entire assembly is heated in an autoclave to cure the epoxy. After the curing process, the multisegmented mandrel is disassembled and removed from inside, leaving the finished tank.

If the tank is to be used for storing hydrogen peroxide, then the liner material should be fluorinated ethylene/propylene (FEP), and one or more FEP O ring(s) should be used in the aluminum end fitting(s). This choice of materials is dictated by experimental observations that pure aluminum and FEP are the only materials suitable for long-term

storage of hydrogen peroxide and that other materials tend to catalyze the decomposition of hydrogen peroxide to oxygen and water.

Other thermoplastic liner materials that are suitable for some applications include nylon 6 and polyethylene. The processing temperatures for nylon 6 are lower than those for FEP. Nylon 6 is compatible with propane, natural gas, and other petroleum-based fuels. Polyethylene is compatible with petroleum-based products and can be used for short-term storage of hydrogen peroxide.

This work was done by Thomas K. DeLay of Marshall Space Flight Center. For further information, access the Technical Support Package (TSP) free on-line at www.techbriefs.com/tsp under the Materials category.

This invention is owned by NASA, and a patent application has been filed. Inquiries concerning nonexclusive or exclusive license for its commercial development should be addressed to the Patent Counsel, Marshall Space Flight Center, (256) 544-0021. Refer to MFS-31401.

Thermally Conductive Metal-Tube/Carbon-Composite Joints

Modified solder joints accommodate differential thermal expansion.

Lyndon B. Johnson Space Center, Houston, Texas

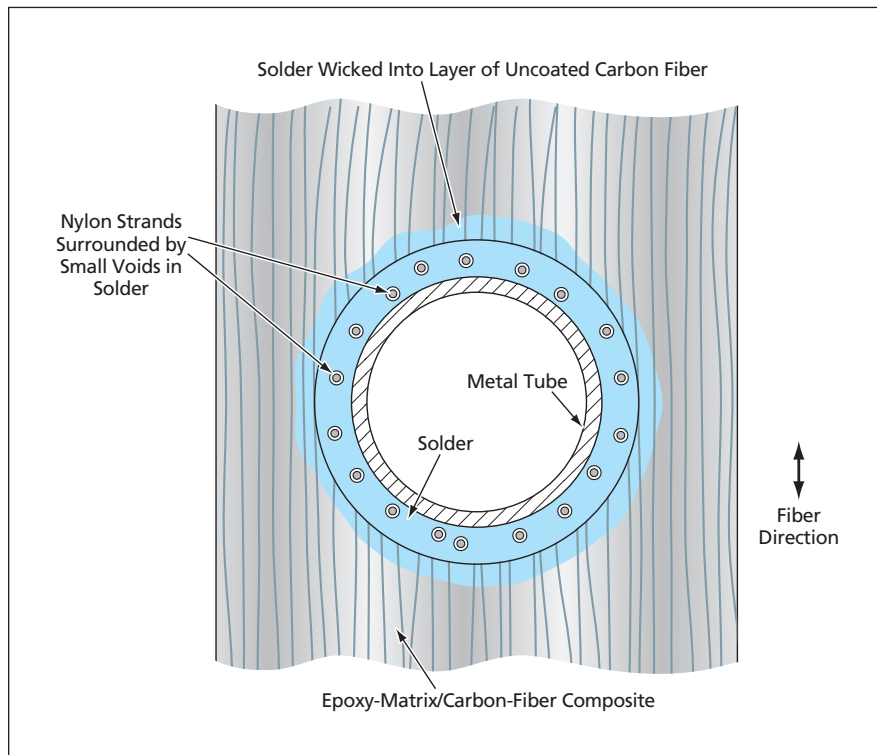
An improved method of fabricating joints between metal and carbon-fiber-based composite materials in lightweight radiators and heat sinks has been devised. Carbon-fiber-based composite materials have been used in such heat-transfer devices because they offer a combination of high thermal conductivity and low mass density. Metal tubes are typically used to carry heat-transfer fluids to and from such heat-transfer de-

vices. The present fabrication method helps to ensure that the joints between the metal tubes and the composite-material parts in such heat-transfer devices have both (1) the relatively high thermal conductances needed for efficient transfer of heat and (2) the flexibility needed to accommodate differences among thermal expansions of dissimilar materials in operation over wide temperature ranges.

Techniques used previously to join metal tubes with carbon-fiber-based composite parts have included press fitting and bonding with epoxy. Both of these prior techniques have been found to yield joints characterized by relatively high thermal resistances.

The present method involves the use of a solder (63 percent Sn, 37 percent Pb) to form a highly thermally conductive joint between a metal tube and a carbon-fiber-based composite structure. Ordinarily, the large differences among the coefficients of thermal expansion of the metal tube, solder, and carbon-fiber-based composite would cause the solder to pull away from the composite upon post-fabrication cooldown from the molten state. In the present method, the structure of the solder is modified (see figure) to enable it to deform readily to accommodate the differential thermal expansion.

In fabricating the composite-material structure, the parts of the carbon fibers adjacent to the hole into which the metal pipe is to be inserted are not coated with the epoxy or other matrix material. The hole is made wide enough to accommodate the tube plus a layer of low-density nylon netting between the tube and the inner surface of the hole. The tube and nylon netting are inserted in the hole, then the solder is melted around the tube. The omission of coating on the fibers adjacent to the hole makes it possible for the solder to wick into the spaces between the fibers and form intimate thermal con-



Small Gaps between the nylon netting and the solder provide flexibility to accommodate differential thermal expansion.

tacts with the fibers. Because the solder does not wet the nylon, a small void forms between each nylon strand and the solder. The thin solder walls that bound the voids are much more flexible than a solid mass of solder would

be; hence, after solidification, the solder can deform to accommodate differential thermal expansion of the various materials present.

This work was done by Robert J. Copeland of TDA Research, Inc., for Johnson Space

Center. For further information, contact:
*TDA Research, Inc.
 12345 W. 52nd Ave.
 Wheat Ridge, CO 80033-1917
 http://www.tda.com
 Refer to MSC-22907.*

Improved BN Coatings on SiC Fibers in SiC Matrices

Outside debonding would be favored over inside debonding.

John H. Glenn Research Center, Cleveland, Ohio

Modifications of BN-based coatings that are used as interfacial layers between the fibers and matrices of SiC-fiber/SiC-matrix composite materials have been investigated to improve the thermomechanical properties of these materials. Such interfacial coating layers, which are also known as interphases (not to be confused with “interphase” in the biological sense), contribute to strength and fracture toughness of a fiber/matrix composite material by providing for limited amounts of fiber/matrix debonding and sliding to absorb some of the energy that would otherwise contribute to the propagation of cracks.

Heretofore, the debonding and sliding have been of a type called “inside debonding” because they have taken place predominantly on the inside surfaces of the BN layers — that is, at the in-

terfaces between the SiC fibers and the interphases. The modifications cause the debonding and sliding to include more of a type, called “outside debonding,” that takes place at the outside surfaces of the BN layers — that is, at the interfaces between the interphases and the matrix (see figure).

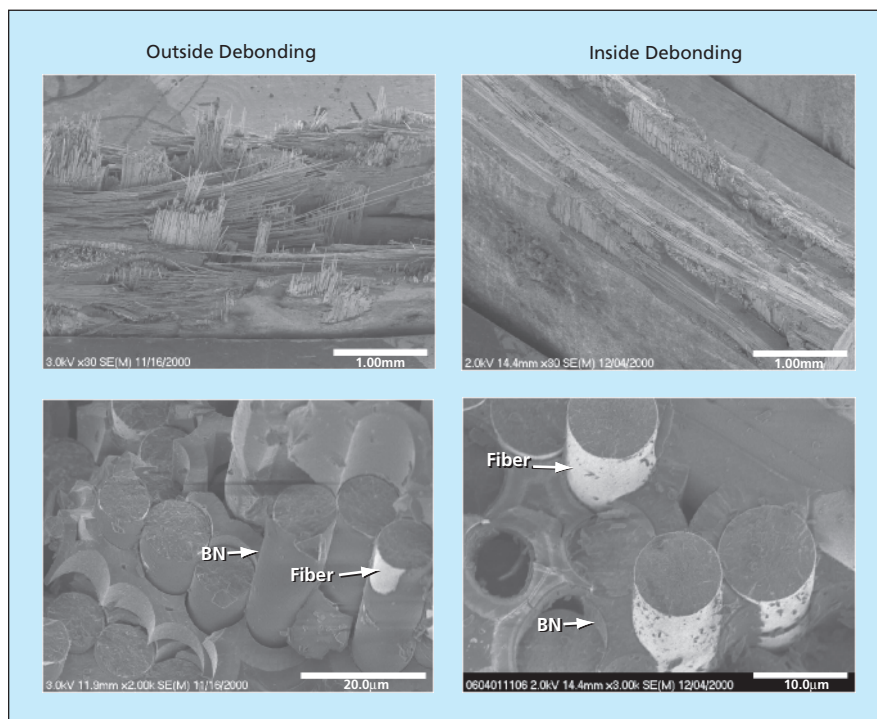
One of the expected advantages of outside debonding is that unlike in inside debonding, the interphases would remain on the crack-bridging fibers. The interphases thus remaining should afford additional protection against oxidation at high temperature and should delay undesired fiber/fiber fusion and embrittlement of the composite material. A secondary benefit of outside debonding is that the interphase/matrix interfaces could be made more compliant than are the fiber/interphase inter-

faces, which necessarily incorporate the roughness of the SiC fibers. By properly engineering BN interphase layers to favor outside debonding, it should be possible, not only to delay embrittlement at intermediate temperatures, but also to reduce the effective interfacial shear strength and increase the failure strain and toughness of the composite material.

Two techniques have been proposed and partially experimentally verified as candidate means to promote outside debonding in state-of-the-art SiC/SiC composites. The first technique is one of application of a weak layer (for example, a layer of C) to the outer surface of the BN interphase. If residual radial tension exists across the interphase (caused, for example, by a thermal-expansion mismatch between the fiber and matrix), then outside debonding could occur during cool down of the composite from its matrix-processing temperature (typically >1,000 °C) to room temperature. If the residual tension is not great enough, outside debonding should nevertheless occur as matrix cracks approach the fibers under some stress conditions.

The second technique for promoting outside debonding is one of heat treatment of the composite at a temperature above that normally used for processing the matrix. During the heat treatment, the BN interphase, which is typically formed in a porous state at temperatures below 1,000 °C, becomes densified by sintering, so that the interphase contracts away from the SiC matrix. This contraction may cause a gap to form between the BN interphase and SiC matrix, or, at the very least, increase the residual radial tension at the BN/matrix interface.

In stress-rupture tests in air at a temperature of 800 °C, the 100-hour failure stress of state-of-the-art SiC/SiC composite modified to promote outside debond-



Specimens of SiC/SiC Composites that have undergone outside and inside debonding are depicted in scanning electron micrographs at various magnifications.

ing was as much as 50 percent greater than that of the corresponding unmodified (inside debonding only) composite. The room-temperature strain to failure of the outside-debonding composite was found to be 0.5 percent, as compared with 0.4 percent for the inside-debonding composite, and the ultimate tensile

strength of the outside-debonding composite was not less than that of the inside-debonding composite.

*This work was done by Gregory N. Morscher, Ramakrishna Bhatt, Hee-Mann Yun, and James A. DiCarlo of **Glenn Research Center**. Further information is contained in a TSP (see page 1).*

Inquiries concerning rights for the commercial use of this invention should be addressed to NASA Glenn Research Center, Commercial Technology Office, Attn: Steve Fedor, Mail Stop 4-8, 21000 Brookpark Road, Cleveland, Ohio 44135. Refer to LEW-17240-1.



Iterative Demodulation and Decoding of Non-Square QAM

The memory inherent in a non-square 2^{2n+1} -QAM can be exploited to obtain coding gains.

NASA's Jet Propulsion Laboratory, Pasadena, California

It has been shown that a non-square (NS) 2^{2n+1} -ary (where n is a positive integer) quadrature amplitude modulation [(NS) 2^{2n+1} -QAM] has inherent memory that can be exploited to obtain coding gains. Moreover, it should not be necessary to build new hardware to realize these gains.

The present scheme is a product of theoretical calculations directed toward reducing the computational complexity of decoding coded 2^{2n+1} -QAM. In the general case of 2^{2n+1} -QAM, the signal constellation is not square and it is impossible to have independent in-phase (I) and quadrature-phase (Q) mapping and demapping. However, independent I and Q mapping and demapping are desirable for reducing the complexity of computing the log likelihood ratio (LLR) between a bit and a received symbol (such computations are essential operations in iterative decoding). This is because in modulation schemes that include independent I and Q mapping and demapping, each bit of a signal point is involved in only one-dimensional mapping and demapping. As a result, the computation of the LLR is equivalent to that of a one-dimensional pulse amplitude modulation (PAM) system. Therefore, it is desirable to find a signal constellation that enables independent I and Q mapping and demapping for 2^{2n+1} -QAM.

Careful labeling of each symbol in the constellation reveals the memory inherent in the corresponding modulation scheme. To obtain the signal constellation or (NS) 2^{2n+1} -QAM, one starts with the square constellation for (NS) 2^{2n+2} -QAM

with independent I-dimension and Q-dimension Gray-code (GC) mapping. That is, each dimension of the square 2^{2n+2} -QAM is an independent PAM with GC mapping. There are 2^{2n+2} signal points in the square 2^{2n+2} -QAM constellation. The GC label of each signal point can be obtained by concatenating its I-dimension GC label with its Q-dimension GC label. If one then deletes every other point in each dimension, then there remain only half of the points in each row and half of the points in each column. The distance between the remaining points in the rows and columns are the same. The total number of remaining points is 2^{2n+1} and these points form the non-square constellation for (NS) 2^{2n+1} -QAM.

The labels of the remaining 2^{2n+1} points are the same as in the square 2^{2n+2} -QAM constellation. This means that $2n+2$ bits are used to label each of the 2^{2n+1} points in the (NS) 2^{2n+1} -QAM constellation: $n+1$ bits for the I-dimension labeling, and $n+1$ bits for the Q-dimension labeling. However, each point in an (NS) 2^{2n+1} -QAM constellation represents only $2n+1$ bits of information. Hence, the $2n+2$ bits used for labeling an (NS) 2^{2n+1} -QAM signal point are not independent.

Close examination has shown that for any signal point in the (NS) 2^{2n+1} -QAM constellation, the last bit of its 2^{n+2} labeling bits can be viewed as a parity-check bit of the other $2n+1$ bits. Therefore, each (NS) 2^{2n+1} -QAM symbol can be generated by first encoding the corresponding $2n+1$ bits with a $(2n+2, 2n+1)$ single-parity-check (SPC) block encoder and then using the $2n+2$ encoded bits to select one of the $2n+1$ points on the (NS) 2^{2n+1} -QAM.

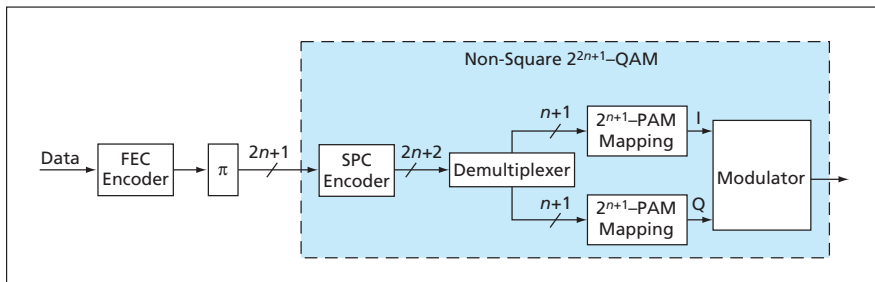
The I-dimension position and the Q-dimension position of a signal point on an (NS) 2^{2n+1} -QAM constellation can be independently determined by the first $n+1$ encoded bits and the remaining $n+1$ encoded bits, respectively. The $(2n+2, 2n+1)$ SPC block code can be generated as a recursive, systematic, terminated convolutional code with two states. In other words, the decomposition of (NS) 2^{2n+1} -QAM into a block encoder and a memoryless modulator leads to a showing that (NS) 2^{2n+1} -QAM is, by itself a form of coded modulation.

When concatenated with a forward-error-correcting (FEC) code (see figure), this decomposition can be applied to obtain joint iterative demodulation and decoding algorithms that exploit the inherent memory of (NS) 2^{2n+1} -QAM so as to achieve better coding gains. In addition, because of the independent I and Q mapping of (NS) 2^{2n+1} -QAM, the decoding complexity can be reduced to that of one-dimensional PAM. Moreover, because the signal constellation of (NS) 2^{2n+1} -QAM is a subset of the square 2^{2n+2} -QAM constellation, it should be possible, in practice, to implement (NS) 2^{2n+1} -QAM by use of 2^{2n+2} -QAM equipment already in existence.

Results of some computational simulations have shown that with iterative demodulation and decoding according to this scheme, coded (NS)8-QAM performs 0.5 dB better than does coded standard 8-QAM and 0.7 dB better than does coded 8-ary phase-shift keying (8 PSK) when the FEC code is the (15,11) Hamming code concatenated with a rate-1 accumulator code. Other simulation results show that coded (NS)32-QAM performs 0.25 dB better than does coded standard 32-QAM.

This work was done by Lifang Li, Dariush Divsalar, and Samuel Dolinar of Caltech for NASA's Jet Propulsion Laboratory. Further information is contained in a TSP (see page 1).

The software used in this innovation is available for commercial licensing. Please contact Don Hart of the California Institute of Technology at (818) 393-3425. Refer to NPO-40308.



A Non-Square 2^{2n+1} -Quadrature Amplitude Modulator would be concatenated with a forward-error-correcting (FEC) encoder. The FEC output bits would be permuted by a random interleaver (π) before each successive group of $2n+1$ bits was mapped into an (NS) 2^{2n+1} -QAM symbol.

Measuring Radiation Patterns of Reconfigurable Patch Antennas on Wafers

Tests can be performed relatively inexpensively and without sawing wafers.

John H. Glenn Research Center, Cleveland, Ohio

An apparatus and technique have been devised for measuring the radiation pattern of a microwave patch antenna that is one of a number of identical units that have been fabricated in a planar array on a high-resistivity silicon wafer. The apparatus and technique are intended, more specifically, for application to such an antenna that includes a DC-controlled microelectromechanical system (MEMS) actuator for switching the antenna between two polarization states or between two resonance frequencies.

Prior to the development of the present apparatus and technique, patch antennas on wafers were tested by techniques and equipment that are more suited to testing of conventional printed-circuit antennas. The techniques included sawing of the wafers to isolate individual antennas for testing. The equipment included custom-built test fixtures that included special signal launchers and transmission-line transitions. The present apparatus and technique eliminate the need for sawing wafers and for custom-built test fixtures, thereby making it possible to test antennas in less time and at less cost. Moreover, in a production setting, elimination of the premature sawing of wafers for testing reduces loss from breakage, thereby enhancing yield.

The apparatus includes (1) a commercial coplanar-waveguide ground-signal-ground radio-frequency (RF) probe, through which microwave excitation is applied to a microstrip transmission line that is part of the integrated circuitry of the patch antenna under test; (2) DC probes for biasing the microelectromechanical actuator; (3) a spinning linearly polarized antenna for sampling the linearly and circularly polarized radiation from the patch antenna as a function of angle relative to the perpendicular to the plane of the wafer; and (4) an automatic network analyzer/microwave receiver for measuring the sampled signal. The microwave probe is a commercial unit of the coplanar-waveguide (CPW) ground-ground-signal-ground type. The microwave and DC probes (see Figure 1) are installed in a

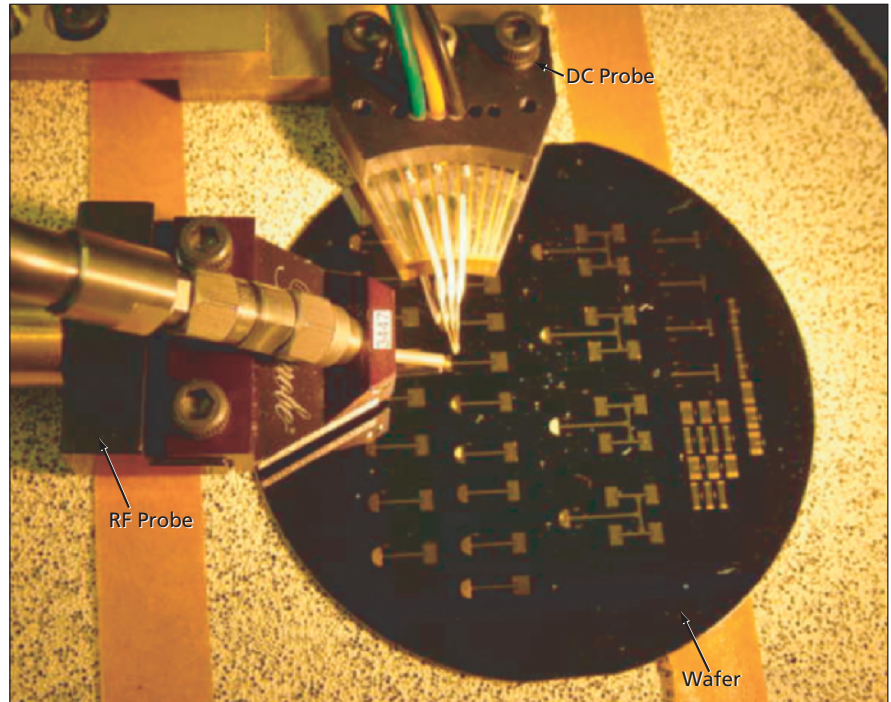


Figure 1. RF and DC Probes are applied to the transmission line of one of several identical patch antennas on a silicon wafer of 3-in. (7.62-cm) diameter.

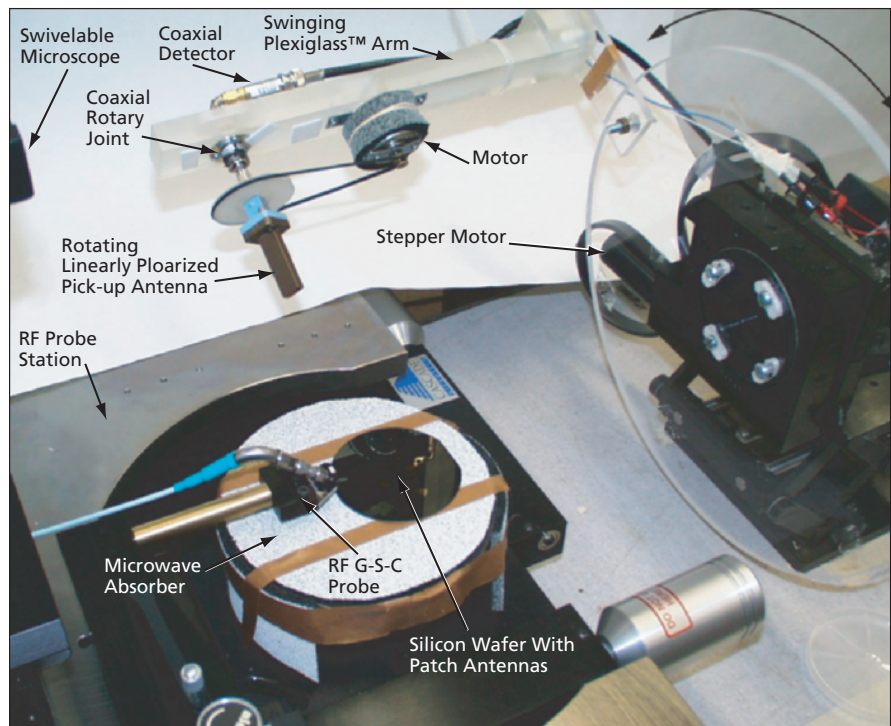


Figure 2. The Spinning Open-Ended Rectangular Waveguide samples the radiation from a patch antenna on the wafer. The antenna is positioned along an arc by use of the stepping motor.

commercial RF wafer probe station that has been modified to accommodate the rotating sampling antenna.

The sampling antenna (see Figure 2) is an open-ended rectangular waveguide that is spun by use of a small DC motor mounted on poly(methyl methacrylate) arm. The signal acquired by the sampling antenna is coupled

through a coaxial rotary joint to a detector that is also mounted on the arm. The arm, in turn, is attached to the shaft of a stepping motor, which is used to position the sampling antenna, in increments of a few degrees, along an arc that extends from -90° to $+90^\circ$ relative to the perpendicular to the plane of the wafer.

This work was done by Rainee N. Simons of Glenn Research Center. Further information is contained in a TSP (see page 1).

Inquiries concerning rights for the commercial use of this invention should be addressed to NASA Glenn Research Center, Commercial Technology Office, Attn: Steve Fedor, Mail Stop 4-8, 21000 Brookpark Road, Cleveland Ohio 44135. Refer to LEW-17462.

Low-Cutoff, High-Pass Digital Filtering of Neural Signals

Digital filtering overcomes the drawbacks of resistor-capacitor filtering.

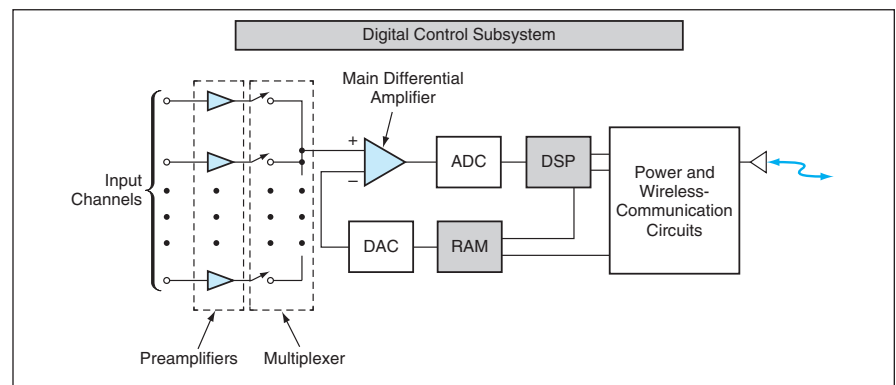
NASA's Jet Propulsion Laboratory, Pasadena, California

The figure depicts the major functional blocks of a system, now undergoing development, for conditioning neural signals acquired by electrodes implanted in a brain. The overall functions to be performed by this system can be summarized as preamplification, multiplexing, digitization, and high-pass filtering.

Other systems under development for recording neural signals typically contain resistor-capacitor analog low-pass filters characterized by cutoff frequencies in the vicinity of 100 Hz. In the application for which this system is being developed, there is a requirement for a cutoff frequency of 5 Hz. Because the resistors needed to obtain such a low cutoff frequency would be impractically large, it was decided to perform low-pass filtering by use of digital rather than analog circuitry. In addition, it was decided to time-multiplex the digitized signals from the multiple input channels into a single stream of data in a single output channel.

The signal in each input channel is first processed by a preamplifier having a voltage gain of approximately 50. Embedded in each preamplifier is a low-pass anti-aliasing filter having a cutoff frequency of approximately 10 kHz. The anti-aliasing filters make it possible to couple the outputs of the preamplifiers to the input ports of a multiplexer. The output of the multiplexer is a single stream of time-multiplexed samples of analog signals. This stream is processed by a main differential amplifier, the output of which is sent to an analog-to-digital converter (ADC). The output of the ADC is sent to a digital signal processor (DSP).

One function of the DSP is to digitally extract the low-frequency component of the signal from each channel (the component that one seeks to filter out) and to store this component in a lookup table [more precisely, a random-access mem-



This **Signal-Conditioning System** is designed to be part of a system for monitoring neural electrical signals. This system implements a low-pass filter having a cutoff frequency of 5 Hz by digital means.

ory (RAM) configured to implement the electronic equivalent of a lookup table]. Another function of the DSP is to assign a gain vector (also stored in the lookup table) for each preamplifier. The gain vector for the preamplifier is presented to the main differential amplifier in synchronism with the arrival of the signal from that preamplifier. This approach prevents the saturation of the main differential amplifier and causes the output signal from every input channel to have optimum strength. Other functions of the DSP include sorting of signal spikes, data compression, and preparation of data for wireless transmission to an external data processor.

The gain of the main differential amplifier is dynamically adjustable. Furthermore, its negative input terminal receives offset signals from the lookup table via a digital-to-analog converter (DAC) for the purpose of subtracting the unwanted low-frequency components of the input signals and thereby performing high-pass filtering. Initial gain and offset values for each channel are determined empirically and stored in the lookup table in a calibration pro-

cedure. During subsequent operation, the offset and gain uniformity of each channel are constantly monitored by use of the combination of the main differential amplifier, ADC, DSP, and lookup table, and the lookup table is periodically refreshed with updated values of the unwanted low-frequency signal components (offsets) and gains.

This work was done by Mohammad Mojarradi, Travis Johnson, Monico Ortiz, Thomas Cunningham, and Richard Andersen of Caltech for NASA's Jet Propulsion Laboratory. Further information is contained in a TSP (see page 1).

In accordance with Public Law 96-517, the contractor has elected to retain title to this invention. Inquiries concerning rights for its commercial use should be addressed to:

*Innovative Technology Assets Management
JPL*

*Mail Stop 202-233
4800 Oak Grove Drive
Pasadena, CA 91109-8099
(818) 354-2240*

E-mail: iaoffice@jpl.nasa.gov

Refer to NPO-30841, volume and number of this NASA Tech Briefs issue, and the page number.

Further Improvement in 3DGRAPE

“3DGRAPE/AL:V2” denotes version 2 of the Three-Dimensional Grids About Anything by Poisson’s Equation with Upgrades from Ames and Langley computer program. The preceding version, 3DGRAPE/AL, was described in “Improved 3DGRAPE” (ARC-14069) *NASA Tech Briefs*, Vol. 21, No. 5 (May 1997), page 66. These programs are so named because they generate volume grids by iteratively solving Poisson’s Equation in three dimensions. The grids generated by the various versions of 3DGRAPE have been used in computational fluid dynamics (CFD). The main novel feature of 3DGRAPE/AL:V2 is the incorporation of an optional scheme in which anisotropic Lagrange-based trans-finite interpolation (ALBTFI) is coupled with exponential decay functions to compute and blend interior source terms. In the input to 3DGRAPE/AL:V2 the user can specify whether or not to invoke ALBTFI in combination with exponential-decay controls, angles, and cell size for controlling the character of grid lines. Of the known programs that solve elliptic partial differential equations for generating grids, 3DGRAPE/AL:V2 is the only code that offers a combination of speed and versatility with most options for controlling the densities and other characteristics of grids for CFD.

This program was written by Stephen Alter of Langley Research Center. Further information is contained in a TSP (see page 1). LAR-16415

Ground Support Software for Spaceborne Instrumentation

ION is a system of ground support software for the ion and neutral mass spectrometer (INMS) instrument aboard the Cassini spacecraft. By incorporating commercial off-the-shelf database, Web server, and Java application components, ION offers considerably more ground-support-service capability than was available previously. A member of the team that operates the INMS or a scientist who uses the data collected by the INMS can gain access to most of the services provided by ION via a standard point-and-click hyperlink interface generated

by almost any Web-browser program running in almost any operating system on almost any computer. Data are stored in one central location in a relational database in a non-proprietary format, are accessible in many combinations and formats, and can be combined with data from other instruments and spacecraft. The use of the Java programming language as a system-interface language offers numerous capabilities for object-oriented programming and for making the database accessible to participants using a variety of computer hardware and software.

This program was written by Vincent Anicich, Rob Thorpe, Greg Fletcher, Hunter Waite, Julia Xu, Erin Walter, Kristie Frick, Greg Farris, Dave Gell, Jufy Furman, Butch Carruth, and John Parejko of Caltech for NASA’s Jet Propulsion Laboratory. Further information is contained in a TSP (see page 1).

This software is available for commercial licensing. Please contact Don Hart of the California Institute of Technology at (818) 393-3425. Refer to NPO-40282.

MER SPICE Interface

MER SPICE Interface is a software module for use in conjunction with the Mars Exploration Rover (MER) mission and the SPICE software system of the Navigation and Ancillary Information Facility (NAIF) at NASA’s Jet Propulsion Laboratory. (SPICE is used to acquire, record, and disseminate engineering, navigational, and other ancillary data describing circumstances under which data were acquired by spaceborne scientific instruments.) Given a Spacecraft Clock value, MER SPICE Interface extracts MER-specific data from SPICE kernels (essentially, raw data files) and calculates values for Planet Day Number, Local Solar Longitude, Local Solar Elevation, Local Solar Azimuth, and Local Solar Time (UTC). MER SPICE Interface was adapted from a subroutine, denoted m98SpiceIF written by Payam Zamani, that was intended to calculate SPICE values for the Mars Polar Lander. The main difference between MER SPICE Interface and m98SpiceIF is that MER SPICE Interface does not explicitly call CHRONOS, a time-conversion program that is part of a library of utility subprograms within SPICE. Instead, MER SPICE Interface mimics some portions of the CHRONOS

code, the advantage being that it executes much faster and can efficiently be called from a pipeline of events in a parallel processing environment.

This program was written by Elias Sayfi of Caltech for NASA’s Jet Propulsion Laboratory. Further information is contained in a TSP (see page 1).

This software is available for commercial licensing. Please contact Don Hart of the California Institute of Technology at (818) 393-3425. Refer to NPO-40314.

Simulating Operation of a Planetary Rover

Rover Analysis, Modeling, and Simulations (ROAMS) is a computer program that simulates the operation of a robotic vehicle (rover) engaged in exploration of a remote planet. ROAMS is a rover-specific extension of the DARTS and Dshell programs, described in prior *NASA Tech Briefs* articles, which afford capabilities for mathematical modeling of the dynamics of a spacecraft as a whole and of its instruments, actuators, and other subsystems. ROAMS incorporates mathematical models of kinematics and dynamics of rover mechanical subsystems, sensors, interactions with terrain, solar panels and batteries, and onboard navigation and locomotion-control software. ROAMS provides a modular simulation framework that can be used for analysis, design, development, testing, and operation of rovers. ROAMS can be used alone for system performance and trade studies. Alternatively, ROAMS can be used in an operator-in-the-loop or flight-software closed-loop environment. ROAMS can also be embedded within other software for use in analysis and development of algorithms, or for Monte Carlo studies, using a variety of terrain models, to generate performance statistics. Moreover, taking advantage of real-time features of the underlying DARTS/Dshell simulation software, ROAMS can also be used for real-time simulations.

This program was written by Abhinandan Jain, Jeng Yen, Garrett Sohl, Robert Steele, and J. Balaram of Caltech for NASA’s Jet Propulsion Laboratory. Further information is contained in a TSP (see page 1).

This software is available for commercial licensing. Please contact Don Hart of the California Institute of Technology at (818) 393-3425. Refer to NPO-30722.

➤ Analyzing Contents of a Computer Cache

The Cache Contents Estimator (CCE) is a computer program that provides information on the contents of level-1 cache of a PowerPC computer. The CCE is configurable to enable simulation of any processor in the PowerPC family. The need for CCE arises because the contents of level-1 caches are not available to either hardware or software readout mechanisms, yet information on the contents is crucial in the development of fault-tolerant or highly available computing systems and for realistic modeling and prediction of computing-system performance. The CCE comprises two independent subprograms: (1) the Dynamic Application Address eXtractor (DAAX), which extracts the stream of address references from an application program undergoing execution and (2) the Cache Simulator (CacheSim), which models the level-1 cache of the processor to be analyzed, by mimicking what the cache controller would do, in response to the address stream from DAAX. CacheSim generates a running estimate of the contents of the data and the instruction sub-caches of the level-1 cache, hit/miss ratios,

the percentage of cache that contains valid or active data, and time-stamped histograms of the cache content.

This program was written by John Beahan, Garen Khanoyan, Raphael Some, and Leslie Callum of Caltech for NASA's Jet Propulsion Laboratory. Further information is contained in a TSP (see page 1). This software is available for commercial licensing. Please contact Don Hart of the California Institute of Technology at (818) 393-3425. Refer to NPO-30669.

➤ Discrepancy Reporting Management System

Discrepancy Reporting Management System (DRMS) is a computer program designed for use in the stations of NASA's Deep Space Network (DSN) to help establish the operational history of equipment items; acquire data on the quality of service provided to DSN customers; enable measurement of service performance; provide early insight into the need to improve processes, procedures, and interfaces; and enable the tracing of a data outage to a change in software or hardware. DRMS is a Web-based software system designed to include a distributed-

database and replication feature to achieve location-specific autonomy while maintaining a consistent high quality of data. DRMS incorporates commercial Web and database software. DRMS collects, processes, replicates, communicates, and manages information on spacecraft data discrepancies, equipment resets, and physical equipment status, and maintains an internal station log. All discrepancy reports (DRs), Master discrepancy reports (MDRs), and Reset data are replicated to a master server at NASA's Jet Propulsion Laboratory; Master DR data are replicated to all the DSN sites; and Station Logs are internal to each of the DSN sites and are not replicated. Data are validated according to several logical mathematical criteria. Queries can be performed on any combination of data.

This program was written by Tonja M. Cooper of Caltech, James C. Lin of Chase Computing International, and Mark L. Chatillon of BAE Systems, Australia, for NASA's Jet Propulsion Laboratory. Further information is contained in a TSP (see page 1).

This software is available for commercial licensing. Please contact Don Hart of the California Institute of Technology at (818) 393-3425. Refer to NPO-30643.



⊕ Silicone-Rubber Microvalves Actuated by Paraffin

Relative to other microvalves, these would be simpler.

NASA's Jet Propulsion Laboratory, Pasadena, California

Microvalves containing silicone-rubber seals actuated by heating and cooling of paraffin have been proposed for development as integral components of microfluidic systems. In comparison with other microvalves actuated by various means (electrostatic, electromagnetic, piezoelectric, pneumatic, and others), the proposed valves (1) would contain simpler structures that could be fabricated at lower cost and (2) could be actuated by simpler (and thus less expensive) control systems.

Each valve according to the proposal would include a flow channel bounded on one side by a flat surface and on the other side by a curved surface defined by an arched-cross-section, elastic seal made of silicone rubber [polydimethylsilane (PDMS)]. The seal would be sized and shaped so that the elasticity of the PDMS would hold the channel open except when the seal was pressed down onto the flat surface to close the channel.

The principle of actuation would exploit the fact that upon melting or freezing, the volume of a typical paraffin increases or decreases, respectively, by about 15 percent. In a valve according to the proposal, the seal face opposite that of the channel would be in contact with a pistonlike plug of paraffin. In the case of a valve designed to be normally open at ambient temperature, one would use a paraffin having a melting temperature above ambient. The seal would be pushed against the flat surface to close the channel by heating the paraffin above its melting temperature. In the case of a valve designed to be normally closed at ambi-

ent temperature, one would use a paraffin having a melting temperature below ambient. The seal would be allowed to spring away from the flat surface to open the channel by cooling the paraffin below its melting temperature. The availability of paraffins that have melting temperatures from -70 to $+80$ °C should make it possible to develop a variety of normally closed and normally open valves.

The figure depicts examples of prototype normally open and normally closed valves according to the proposal. In each valve, an arch cross section defining a channel having dimensions of the order of tens of micrometers would be formed in a silicone-rubber sheet about 40 μm thick. The silicone-rubber sheet would be hermetically sealed to a lower glass plate that would define the sealing surface and to an upper glass plate containing a well. The well would be filled with paraffin and capped with a rigid restraining layer of epoxy. In the normally open valve, the paraffin would have a melting temperature above ambient (e.g., 40 °C) and

the wall of the well would be coated with a layer of titanium that would serve as an electric heater. In the normally closed valve, the paraffin would have a melting temperature below ambient (e.g., -5 °C). Instead of a heater in the well, the normally closed valve would include a thermoelectric cooler on top of the epoxy cap.

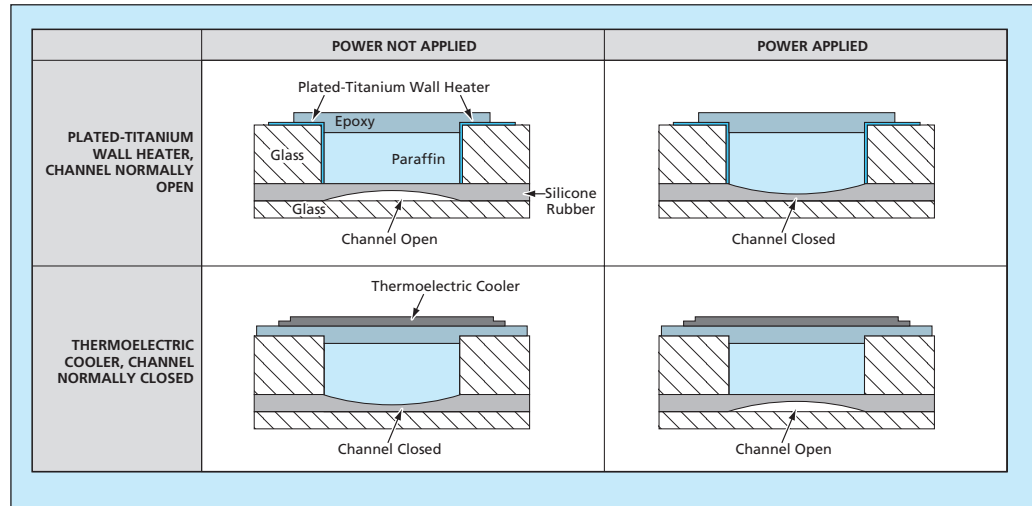
This work was done by Danielle Svelha, Sabrina Feldman, and David Barsic of Caltech for NASA's Jet Propulsion Laboratory. Further information is contained in a TSP (see page 1).

In accordance with Public Law 96-517, the contractor has elected to retain title to this invention. Inquiries concerning rights for its commercial use should be addressed to:

*Innovative Technology Assets Management
JPL*

*Mail Stop 202-233
4800 Oak Grove Drive
Pasadena, CA 91109-8099
(818) 354-2240*

*E-mail: iaoffice@jpl.nasa.gov
Refer to NPO-30519, volume and number of this NASA Tech Briefs issue, and the page number.*



Normally Open and Normally Closed Microvalves would both exploit the large changes in volume of paraffin that occur upon melting and freezing.

Hydraulic Apparatus for Mechanical Testing of Nuts

Advantages include mobility and reduced setup time.

Lyndon B. Johnson Space Center, Houston, Texas

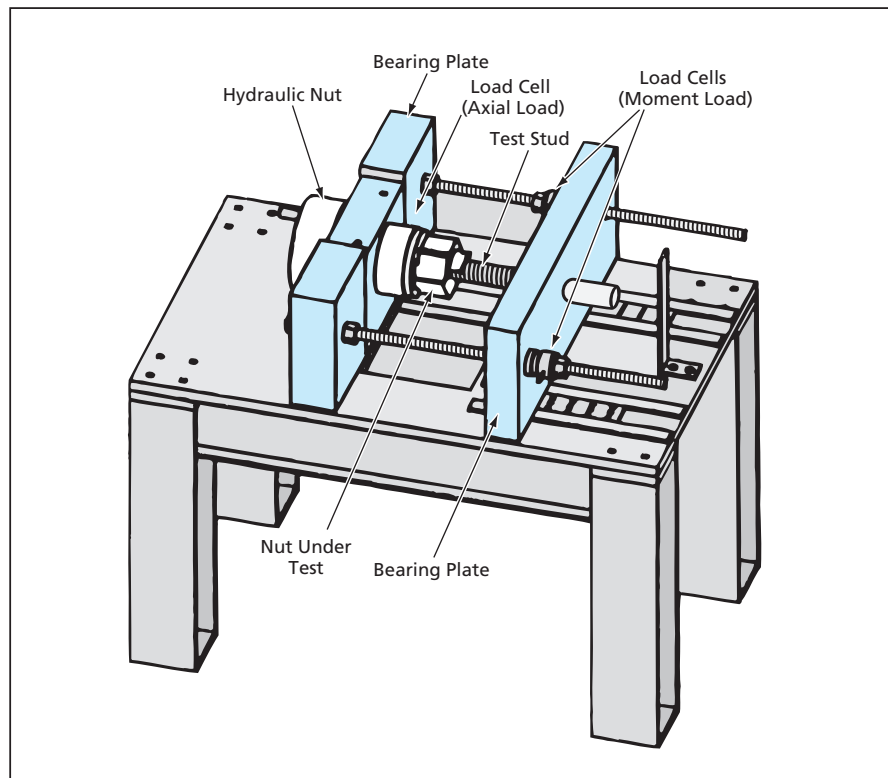
The figure depicts an apparatus for mechanical testing of nuts. In the original application for which the apparatus was developed, the nuts are of a frangible type designed for use with pyrotechnic devices in spacecraft applications in which there are requirements for rapid, one-time separations of structures that are bolted together. The apparatus can also be used to test non-frangible nuts engaged without pyrotechnic devices.

This apparatus was developed to replace prior testing systems that were extremely heavy and immobile and characterized by long setup times (of the order of an hour for each nut to be tested). This apparatus is mobile, and the setup for each test can now be completed in about five minutes.

The apparatus can load a nut under test with a static axial force of as much as 6.8×10^5 lb (3.0 MN) and a static moment of as much as 8.5×10^4 lb-in. (9.6×10^3 N-m) for a predetermined amount of time. In the case of a test of a frangible nut, the pyrotechnic devices can be exploded to break the nut while the load is applied, in which case the breakage of the nut relieves the load. The apparatus can be operated remotely for safety during an explosive test.

The load-generating portion of the apparatus is driven by low-pressure compressed air; the remainder of the apparatus is driven by 110-Vac electricity. From its source, the compressed air is fed to the apparatus through a regulator and a manually operated valve. The regulated compressed air is fed to a pneumatically driven hydraulic pump, which pressurizes oil in a hydraulic cylinder, thereby causing a load to be applied via a hydraulic nut (not to be confused with the nut under test). During operation, the hydraulic pressure is correlated with the applied axial load, which is verified by use of a load cell.

Prior to operation, one end of a test stud (which could be an ordinary



The Hydraulic Unit Applies a Load to the nut under test via the hydraulic nut and the test stud.

threaded rod or bolt) is installed in the hydraulic nut. The other end of the test stud passes through a bearing plate; a load cell is slid onto that end, and then the nut to be tested is threaded onto that end and tightened until the nut and load cell press gently against the bearing plate.

The axial load is applied to the nut under test as the air and hydraulic pressures increase. The manually operated hand valve is closed to isolate the hydraulic pump to hold the load on the test article. A second manually operated valve is used to dump the hydraulic oil back to a reservoir to relieve the load. The maximum axial load is limited by a relief valve on the compressed air source; the maximum load can be changed by adjusting the setting of this valve.

To set up the apparatus to apply a moment load, one adds a second bearing plate, through which the test stud passes with a tight fit. Specific loads can be applied to the second bearing plate by torquing nuts on the all-thread connecting the two bearing plates, at a set distance from the center line of the test stud. These loads are verified by use of load cells. The movement of the second bearing plate creates a bind with the end of the test stud, thereby giving rise to a moment load applied to the nut under test.

This work was done by Todd J. Hinkel, Richard J. Dean, Scott C. Hacker, and Douglas W. Harrington of Johnson Space Center and Frank Salazar of Lockheed Martin. For further information, contact Richard J. Dean at richard.j.dean@nasa.gov. MSC-23159

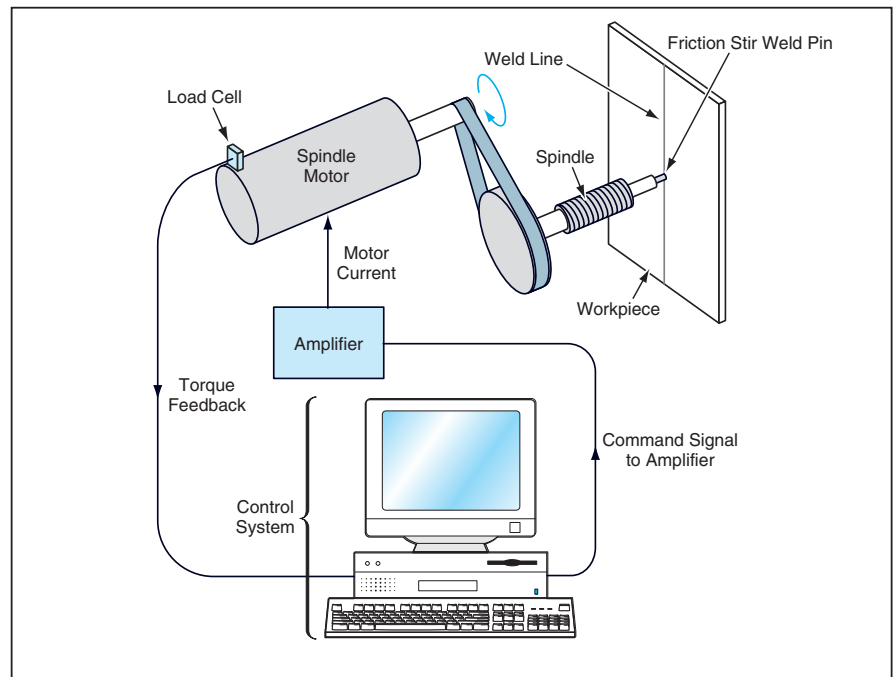
Heat Control via Torque Control in Friction Stir Welding

Torque would be controlled and rotation measured to measure and control heat input.

Marshall Space Flight Center, Alabama

In a proposed advance in friction stir welding, the torque exerted on the workpiece by the friction stir pin would be measured and controlled in an effort to measure and control the total heat input to the workpiece. The total heat input to the workpiece is an important parameter of any welding process (fusion or friction stir welding). In fusion welding, measurement and control of heat input is a difficult problem. However, in friction stir welding, the basic principle of operation affords the potential of a straightforward solution: Neglecting thermal losses through the pin and the spindle that supports it, the rate of heat input to the workpiece is the product of the torque and the speed of rotation of the friction stir weld pin and, hence, of the spindle. Therefore, if one acquires and suitably processes data on torque and rotation and controls the torque, the rotation, or both, one should be able to control the heat input into the workpiece.

In conventional practice in friction stir welding, one uses feedback control of the spindle motor to maintain a constant speed of rotation. According to the proposal, one would not maintain a constant speed of rotation: Instead, one would use feedback control to maintain a constant torque and would measure the speed of rotation while allowing it to vary. The torque exerted on the



The **Motor Current Would Be Regulated** to maintain constant torque, as part of a scheme to measure and/or control the total heat imparted to the motion of the friction stir weld pin.

workpiece would be estimated as the product of (1) the torque-multiplication ratio of the spindle belt and/or gear drive, (2) the force measured by a load cell mechanically coupled to the spindle motor, and (3) the moment of the load cell would be used as a feed-

back signal for controlling the torque (see figure).

This work was done by Richard Venable, Kevin Colligan, and Alan Knapp of Lockheed Martin Corp. for Marshall Space Flight Center. For further information, contact the New Technology Representative, Gary Willett at (504) 257-4786. MFS-31834

Manufacturing High-Quality Carbon Nanotubes at Lower Cost

The cost is about 1/20 of that of other processes.

Goddard Space Flight Center, Greenbelt, Maryland

A modified electric-arc welding process has been developed for manufacturing high-quality batches of carbon nanotubes at relatively low cost. Unlike in some other processes for making carbon nanotubes, metal catalysts are not used and, consequently, it is not necessary to perform extensive cleaning and purification. Also, unlike some other processes, this process is carried out at

atmospheric pressure under a hood instead of in a closed, pressurized chamber; as a result, the present process can be implemented more easily.

Although the present welding-based process includes an electric arc, it differs from a prior electric-arc nanotube-production process. The welding equipment used in this process includes an AC/DC welding power

source with an integral helium-gas delivery system and circulating water for cooling an assembly that holds one of the welding electrodes (in this case, the anode).

The cathode is a hollow carbon (optionally, graphite) rod having an outside diameter of 2 in. (≈ 5.1 cm) and an inside diameter of 5/8 in. (≈ 1.6 cm). The cathode is partly immersed in a water

bath, such that it protrudes about 2 in. (about 5.1 cm) above the surface of the water. The bottom end of the cathode is held underwater by a clamp, to which is connected the grounding cable of the welding power source.

The anode is a carbon rod 1/8 in. (≈ 0.3 cm) in diameter. The assembly that holds the anode includes a thumb-knob-driven mechanism for controlling the height of the anode. A small hood is placed over the anode to direct a flow of helium downward from the anode to the cathode during the welding process. A bell-shaped exhaust hood collects the helium and other gases from the process. During the process, as the anode is consumed, the height of the

anode is adjusted to maintain an anode-to-cathode gap of 1 mm.

The arc-welding process is continued until the upper end of the anode has been lowered to a specified height above the surface of the water bath. The process causes carbon nanotubes to form in the lowest 2.5 cm of the anode. It also causes a deposit reminiscent of a sandcastle to form on the cathode. The nanotube-containing material is harvested. The cathode and anode can then be cleaned (or the anode is replaced, if necessary) and the process repeated to produce more nanotubes.

Tests have shown that the process results in ≈ 50 -percent yield of carbon nanotubes (mostly of the single-wall

type) of various sizes. Whereas the unit cost of purified single-wall carbon nanotubes produced by other process is about \$1,000/g in the year 2000, it has been estimated that for the present process, the corresponding cost would be about \$10/g.

*This work was done by Jeanette M. Benavides and Henning Lidecker of **Goddard Space Flight Center**. Further information is contained in a TSP (see page 1).*

This invention has been patented by NASA (U.S. Patent No. 6,114,995). Inquiries concerning nonexclusive or exclusive license for its commercial development should be addressed to the Patent Counsel, Goddard Space Flight Center; (301) 286-7351. Refer to GSC-14601.

Setup for Visual Observation of Carbon-Nanotube Arc Process

Lyndon B. Johnson Space Center, Houston, Texas

A simple optical setup has been devised to enable safe viewing of the arc and measurement of the interelectrode gap in a process in which carbon nanotubes are produced in an arc between a catalyst-filled carbon anode and a graphite cathode. This setup can be used for visually guided manual positioning of the anode to maintain the interelectrode gap at a desired constant value, possibly as a low-technology alternative to the automatic position/voltage

control described in "Automatic Control of Arc Process for Making Carbon Nanotubes" (MSC-23134), *NASA Tech Briefs*, Vol. 28, No. 3 (March 2004), page 51. The optical setup consists mainly of lenses for projecting an image of the arc onto a wall, plus a calibrated grid that is mounted on the wall so that one can measure the superimposed image of the arc. To facilitate determination of the end point of the process, the anode is notched, by use of a file, at the end of

the filled portion that is meant to be consumed in the process. As the anode is consumed and the notch comes into view in the scene projected onto the wall, the process operator switches off the arc current.

*This work was done by Carl D. Scott of **Johnson Space Center** and Sivaram Arepalli of GB Tech Inc. For further information, contact the Johnson Commercial Technology Office at (281) 483-3809. MSC-23131*



Solution Preserves Nucleic Acids in Body-Fluid Specimens

Specimens can be stored and transported at room temperature.

Lyndon B. Johnson Space Center, Houston, Texas

A solution has been formulated to preserve deoxyribonucleic acid (DNA) and ribonucleic acid (RNA) in specimens of blood, saliva, and other bodily fluids. Specimens of this type are collected for diagnostic molecular pathology, which is becoming the method of choice for diagnosis of many diseases. The solution makes it possible to store such specimens at room temperature, without risk of decomposition, for subsequent analysis in a laboratory that could be remote from the sampling location. Thus, the solution could be a means to bring the benefits of diagnostic molecular pathology to geographic regions where refrigeration equipment and diagnostic laboratories are not available.

The table lists the ingredients of the solution. The functions of the ingredients are the following:

- EDTA chelates divalent cations that are necessary cofactors for nuclease activity. In so doing, it functionally removes these cations and thereby retards the action of nucleases. EDTA also stabilizes the DNA helix.
- Tris serves as a buffering agent, which is needed because minor contaminants in an unbuffered solution can exert pronounced effects on pH and

Ingredient	Weight or Volume of Ingredient	Final Concentration of Ingredient in Solution
Sodium dodecyl sulfate (SDS)	1 g	1 percent
Ethylenediaminetetraacetic acid (EDTA)	0.037 g	1.0 mM
Tris(hydroxymethyl)aminomethane (also known as "Tris" and sold under the trade name Trizma™ Base)	0.12 g	10 mM
Water Free of Deoxyribonuclease and Ribonuclease	99 mL	
	Total Volume 100 mL	

The **Nucleic Acid Stability Solution (NASS)** contains ingredients that perform different roles essential to the preservation of DNA and RNA in specimens. In the preparation of this solution, the ingredients are mixed in the indicated quantities (or common multiples thereof), then the solution is sterilized by passing it through a 0.2- μ m filter.

thereby cause spontaneous degradation of DNA.

- SDS is an ionic detergent that inhibits ribonuclease activity. SDS has been used in some lysis buffers and as a storage buffer for RNA after purification.

The use of the solution is straightforward. For example, a sample of saliva is collected by placing a cotton roll around in the subject's mouth until it becomes saturated, then the cotton is placed in a collection tube. Next, 1.5 mL of the solution are injected directly

into the cotton and the tube is capped for storage at room temperature. The effectiveness of the solution has been demonstrated in tests on specimens of saliva containing herpes simplex virus. In the tests, the viral DNA, as amplified by polymerase chain reaction, was detected even after storage for 120 days.

This work was done by Duane L. Pierson of Johnson Space Center and Raymond P. Stowe. For further information, contact the Johnson Commercial Technology Office at (281) 483-3809. MSC-22891

Oligodeoxynucleotide Probes for Detecting Intact Cells

Cells can be detected, identified, and enumerated via chemiluminescence.

Lyndon B. Johnson Space Center, Houston, Texas

A rapid, sensitive test using chemiluminescent oligodeoxynucleotide probes has been developed for detecting, identifying, and enumerating intact cells. The test is intended especially for use in detecting and enumerating bacteria and yeasts in potable water.

As in related tests that have been developed recently for similar purposes, the oligodeoxynucleotide probes used in this test are typically targeted at either single-copy deoxyribonucleic acid (DNA) genes (such as virulence genes) or the multiple

copies (10,000 to 50,000 copies per cell) of 16S ribosomal ribonucleic acids (rRNAs). Some of those tests involve radioisotope or fluorescent labeling of the probes for reporting hybridization of probes to target nucleic acids. Others of those tests involve labeling with enzymes plus the use of chemiluminescent or chromogenic substrates to report hybridization via color or the emission of light, respectively. The present test is of the last-mentioned type. The chemiluminescence in the present test can be detected easily with relatively sim-

ple instrumentation.

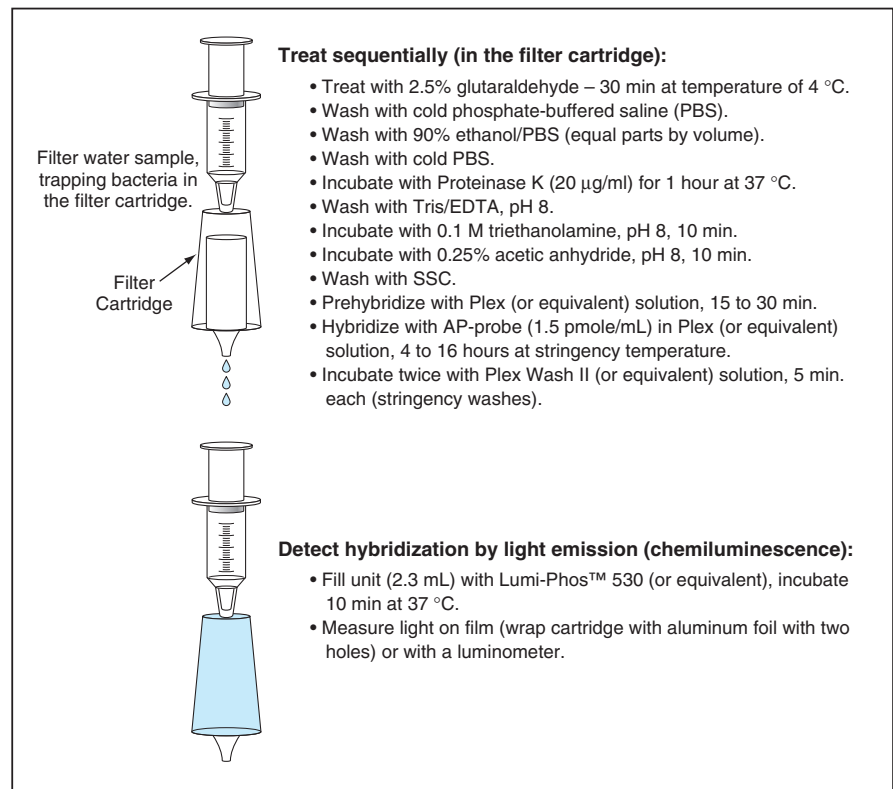
In developing the present test, the hybridization approach was chosen because hybridization techniques are very specific. Hybridization detects stable, inheritable genetic targets within microorganisms. These targets are not dependent on products of gene expression that can vary with growth conditions or physiological states of organisms in test samples. Therefore, unique probes can be designed to detect and identify specific genera or species of bacteria or

yeast (in terms of rRNA target sequences) or can be designed to detect and identify virulence genes (genomic target sequences). Because of the inherent specificity of this system, there are few problems of cross-reactivity.

Hybridization tests are rapid, but hybridization tests now available commercially lack sensitivity; typically, between 10^6 and 10^7 cells of the target organism are needed to ensure a reliable test. Consequently, the numbers of target bacteria in samples are usually amplified by overnight pre-enrichment growth. These tests are usually performed in laboratories by skilled technicians. The present test was designed to overcome the shortcomings of the commercial hybridization tests.

The figure summarizes the major steps of the test. It is important to emphasize that the hybridization process used in this test differs from that of other hybridization tests in that it does not extract target nucleic acids. This process is based on intact-cell hybridization (so-called "in situ hybridization"), wherein the intact cells act as immobilizing agents. The cells are identified and enumerated by measuring the chemiluminescence emitted from alkaline phosphatase-probe (AP-probe) hybridization; the chemiluminescence is detected or measured by use of photographic film or a luminometer, respectively.

This test provides rapid, simple, and sensitive detection of microorganisms in water. The test is very flexible: specific probes can be developed for almost any group, genus, and, in many cases, species of microorganisms. The



Treat sequentially (in the filter cartridge):

- Treat with 2.5% glutaraldehyde – 30 min at temperature of 4 °C.
- Wash with cold phosphate-buffered saline (PBS).
- Wash with 90% ethanol/PBS (equal parts by volume).
- Wash with cold PBS.
- Incubate with Proteinase K (20 µg/ml) for 1 hour at 37 °C.
- Wash with Tris/EDTA, pH 8.
- Incubate with 0.1 M triethanolamine, pH 8, 10 min.
- Incubate with 0.25% acetic anhydride, pH 8, 10 min.
- Wash with SSC.
- Prehybridize with Plex (or equivalent) solution, 15 to 30 min.
- Hybridize with AP-probe (1.5 pmole/mL) in Plex (or equivalent) solution, 4 to 16 hours at stringency temperature.
- Incubate twice with Plex Wash II (or equivalent) solution, 5 min. each (stringency washes).

Detect hybridization by light emission (chemiluminescence):

- Fill unit (2.3 mL) with Lumi-Phos™ 530 (or equivalent), incubate 10 min at 37 °C.
- Measure light on film (wrap cartridge with aluminum foil with two holes) or with a luminometer.

Intact-Cell Hybridization is performed in a filter cartridge using chemiluminescent oligodeoxynucleotide probes to detect target bacteria.

test can be performed in the field, or in a laboratory, using simple, battery-powered portable instrumentation. The test can be initiated and completed by non-technical persons. The test format can be automated easily. Probes for *E. coli* and the coliform group of bacteria have been developed for testing water. Results of a test can be obtained within 8 hours. Probes for *Vibrio cholerae*, *Burkholderia cepacia*, *Staphylococcus aureus*,

Staphylococcus epidermidis, and the *Salmonella* group have also been developed.

This work was done by Reinhardt A. Rosson, Julie Mawrina-Brunker, Kim Langley, and Christine M. Pynnönen of Bio-Technical Resources, L. P. for Johnson Space Center. For further information, contact the Johnson Commercial Technology Office at (281) 483-3809. MSC-22663



Microwave-Spectral Signatures Would Reveal Concealed Objects

This technique should prove superior to conventional ground-probing radar.

Lyndon B. Johnson Space Center, Houston, Texas

A proposed technique for locating concealed objects (especially small antipersonnel land mines) involves the acquisition and processing of spectral signatures over broad microwave frequency bands. This technique was conceived to overcome the weaknesses of older narrow-band electromagnetic techniques like ground-probing radar and low-frequency electromagnetic induction.

Ground-probing radar is susceptible to false detections and/or interference caused by rocks, roots, air pockets, soil inhomogeneities, ice, liquid water, and miscellaneous buried objects other than those sought. Moreover, if the radar frequency happens to be one for which the permittivity of a sought object matches the permittivity of the surrounding soil or there is an unfavorable complex-amplitude addition of the radar reflection at the receiver, then the object is not detected. Low-frequency electromagnetic induction works well for detecting metallic objects, but the amounts of metal in plastic mines are often too small to be detectable.

The potential advantage of the proposed technique arises from the fact that wideband spectral signatures generally contain more relevant information than do narrow-band signals. Consequently, spectral signatures could be used to make better decisions regarding whether concealed objects are present and whether they are the ones sought. In some cases, spectral signatures could provide information on the depths, sizes, shapes, and compositions of objects.

An apparatus to implement the proposed technique (see Figure 1) could be assembled from equipment already in common use. Typically, such an apparatus would include a radio-frequency (RF) transmitter/receiver, a broad-band microwave antenna, and a fast personal computer loaded with appropriate software. In operation, the counter would be turned on, the antenna would be aimed at the ground or other mass suspected to contain a mine or other sought object, and the operating frequency would be swept over the band of interest.

For success in detection, (1) at least a small portion of the electromagnetic wave radiated by the antenna must penetrate the soil or other mass, must impinge on the sought object, and must be

either scattered or reflected back to the antenna; and (2) there must be a suitable frequency-dependent mismatch of impedances, as explained next: If, for example, the object sought were a plas-

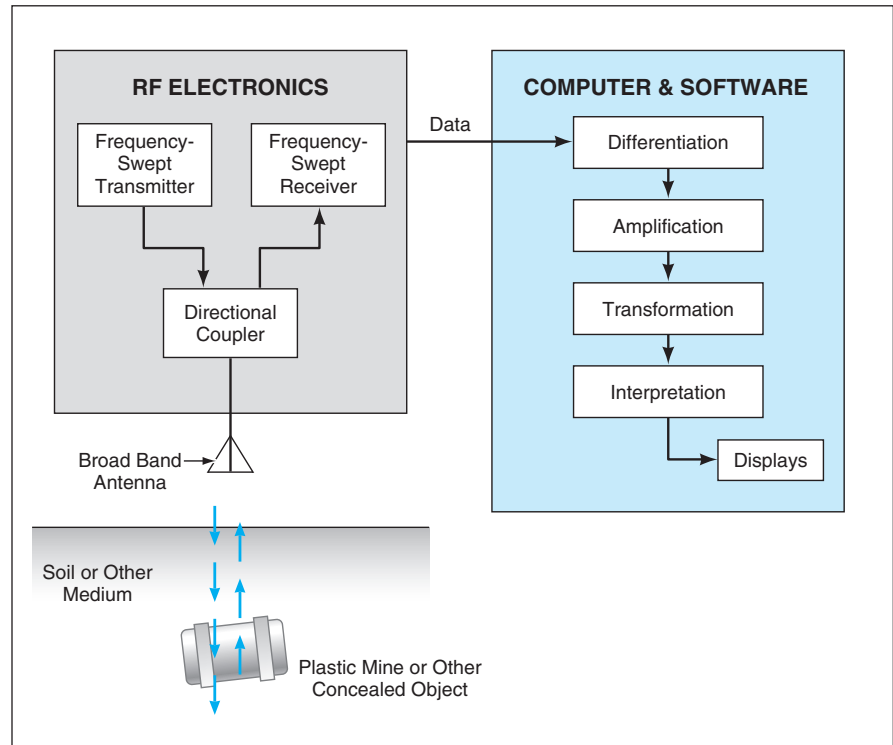


Figure 1. Microwave Reflections From the Concealed Object would contribute to the frequency-dependent input impedance of the antenna. The impedance would be measured by the network analyzer, and the frequency dependence would be processed to extract information about the concealed object.

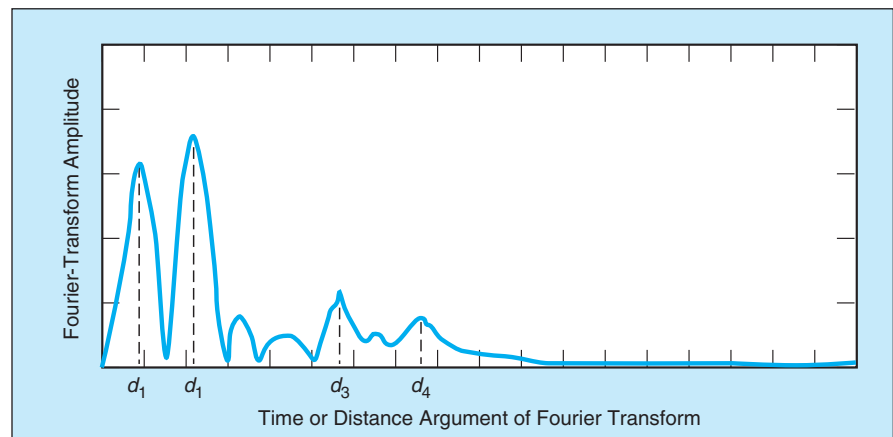


Figure 2. This Plot Is the Fourier Transform of a processed spectral signature, calculated theoretically for the case of a small buried plastic mine.

tic mine or other dielectric object, then some microwave energy would penetrate the object, would undergo one or more internal reflections, and would then be scattered or reflected back toward the antenna. The magnitude and phase of each of these reflections would depend on frequency and would contribute to the spectral signature of the object and the surrounding material. The spectral signature would manifest itself as the frequency dependence of the input impedance of the antenna. This impedance would be measured by the computer.

The impedance-vs.-frequency data must be processed to extract useful information on the location and nature of the sought object. One algorithm that could be used for this purpose can be summarized as follows:

1. Proceeding across the frequency band, calculate a running average of

the magnitude of input impedance vs. frequency.

2. Compute the difference between the magnitude of impedance and the running average at each frequency.
3. Uniformly digitally amplify the difference data for all frequencies over the band.
4. Compute the Fourier transform of the difference-vs.-frequency data to obtain a plot that is intuitively easy to interpret because its abscissa is proportional to time and is thus related to signal-propagation distance and permittivity.

Figure 2 presents such a plot calculated theoretically for an apparatus operating in the frequency band of 1 to 10 GHz with its antenna aimed toward soil in which a plastic mine 3 in. (7.6 cm) in diameter and 1-1/2 in. (3.8 cm) thick is buried. The first spectral peak is caused by reflection of the microwave signal

from the antenna input terminal and is located at d_1 , which is proportional to the length of a coaxial cable from the network analyzer to the antenna. The second peak, located at d_2 , is associated with the reflection of the microwave signal at the surface of the ground. The largest next two peaks, located at d_3 and d_4 , are attributable to reflection from the top and bottom surfaces of the mine; thus, d_3 and d_4 are measures of the depth of burial of the mine.

This work was done by G. Arndt and P. Ngo of Johnson Space Center, J. R. Carl of Lockheed Martin, and K. Byerly and L. Stolarczyk.

This invention is owned by NASA, and a patent application has been filed. Inquiries concerning nonexclusive or exclusive license for its commercial development should be addressed to the Patent Counsel, Johnson Space Center, (281) 483-0837. Refer to MSC-22839.

Digital Averaging Phasemeter for Heterodyne Interferometry

One instrument performs functions for which separate instruments were previously needed.

NASA's Jet Propulsion Laboratory, Pasadena, California

A digital averaging phasemeter has been built for measuring the difference between the phases of the unknown and reference heterodyne signals in a heterodyne laser interferometer. This phasemeter performs well enough to enable interferometric measurements of distance with accuracy of the order of 100 pm and with the ability to track distance as it changes at a speed of as much as 50 cm/s. This phasemeter is unique in that it is a single, integral system capable of performing three major functions that, heretofore, have been performed by separate systems: (1) measurement of the fractional-cycle phase difference, (2) counting of multiple cycles of phase change, and (3) averaging of phase measurements over multiple cycles for improved resolution. This phasemeter also offers the advantage of making repeated measurements at a high rate: the phase is measured on every heterodyne cycle. Thus, for example, in measuring the relative phase of two signals having a heterodyne frequency of 10 kHz, the phasemeter would accumulate 10,000 measurements per second. At this high measurement rate, an accurate average phase determination can be made more quickly than is possible at a lower rate.

Figure 1 schematically depicts a typi-

cal heterodyne laser interferometer in which the phasemeter is used. The goal is to measure the change in the length of the optical path between two corner cube retroreflectors. Light from a stabilized laser is split into two fiber-optic outputs, denoted P and S, respectively, that are mutually orthogonally polarized and separated by a well-defined heterodyne frequency. The two fiber-optic outputs

are fed to a beam launcher that, along with the corner-cube retroreflectors, is part of the interferometer optics. In addition to launching the beams, the beam launcher immediately diverts and mixes about 10 percent of the power from the fiber-optic feeds to obtain a reference heterodyne signal. This signal is detected, amplified, and squared to obtain a reference square-wave heterodyne sig-

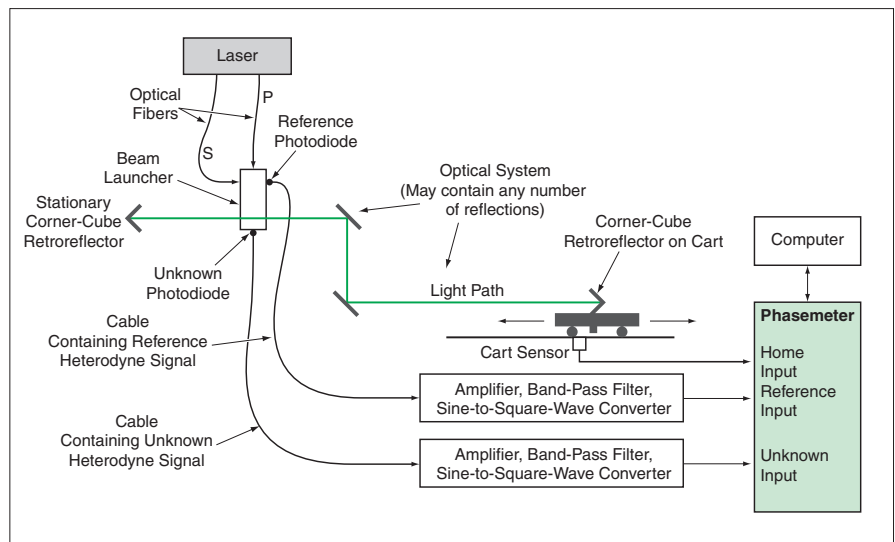


Figure 1. A Heterodyne Laser Interferometer is used to measure changes in the length of the optical path between the corner-cube retroreflectors. These changes are proportional to changes in the phase difference between the reference and unknown signals, which are measured by the phasemeter.

nal, which is fed to the reference input terminal of the phasemeter.

The remaining 90 percent of the power from the fiber-optic feeds of the light from the two inputs is treated as follows: The P beam is launched toward one corner-cube retroreflector, while the S beam travels to the unknown photodiode. The S beam returns to the beam launcher, passes through it, and continues to the other retroreflector. The S beam then returns to the beam launcher where it mixes with the P beam, producing the "unknown" heterodyne signal, which is then detected, amplified, and

squared in the same manner as that of the reference signal. The resulting square-wave is fed to the unknown input terminal of the phasemeter.

The frequency of the unknown heterodyne signal is close to that of the reference signal: If the optics are motionless, the unknown frequency is exactly the reference frequency. Motion of the optics gives rise to a Doppler shift in the unknown frequency relative to the reference frequency. By tracking the relative phases of the unknown and reference signals, one tracks the change in the length of the optical path between the retroreflectors.

The phasemeter (see Figure 2) tracks the integer number of cycles and the fractional-cycle portions of the phase difference separately. The integer part of the phase difference is taken to equal the number of positive- or negative-going square-wave level transitions at the reference input minus the number of such transitions at the unknown input. The fractional part of the phase difference is taken to be proportional to the number of ticks of a clock of 128-MHz frequency during the time interval from the most recent reference transition to the next unknown transition.

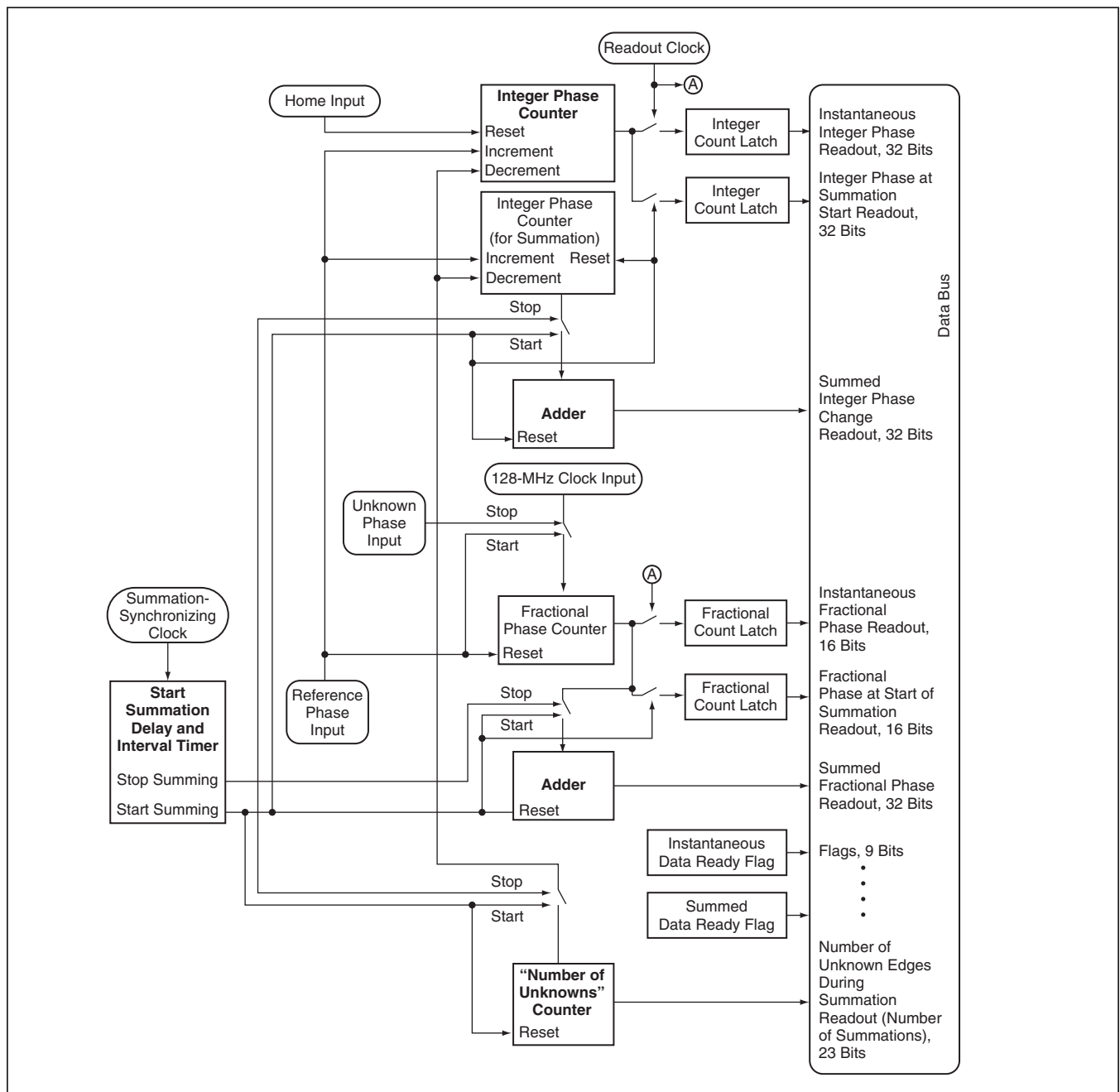


Figure 2. In the Phasemeter, the integer-cycle and fractional-cycle parts of the phase difference are measured separately. For greater accuracy, the phasemeter can average its measurements over many cycles of the heterodyne signals.

The integer and fractional phase-counter outputs are also fed to accumulators to compute the sum of many phase measurements over a programmed interval. The sum is then used to compute an average. The summing interval can be made to repeat at a fixed frequency, typically in the range between 1 Hz and 1 kHz, that is defined by a signal from a summation-synchronizing clock. The averaging interval can be programmed to

start any time after the summation-synchronizing clock signal and can continue for any time up to the next such signal. During the summation, each negative-going transition of the unknown signal causes a phase measurement to be summed into the integer and fractional phase accumulators. As a result, the number of readings in an average equals the duration of the summation interval multiplied by the unknown heterodyne

frequency; for example, if the heterodyne frequency is 10 kHz and the summation interval is 0.1 second, then 1,000 measurements are accumulated.

*This work was done by Donald Johnson, Robert Spero, Stuart Shaklan, Peter Halverson, and Andreas Kuhnert of Caltech for NASA's Jet Propulsion Laboratory. Further information is contained in a TSP (see page 1).
NPO-30866*

Optoelectronic Instrument Monitors pH in a Culture Medium

This instrument is noninvasive and is not significantly affected by biofilm.

Lyndon B. Johnson Space Center, Houston, Texas

An optoelectronic instrument monitors the pH of an aqueous cell-culture medium in a perfused rotating-wall-vessel bioreactor. The instrument is designed to satisfy the following requirements:

- It should be able to measure the pH of the medium continuously with an accuracy of ± 0.1 in the range from 6.5 to 7.5.
- It should be noninvasive.
- Any material in contact with the culture medium should be sterilizable as well as nontoxic to the cells to be grown in the medium.
- The biofilm that inevitably grows on any surface in contact with the medium should not affect the accuracy of the pH measurement.
- It should be possible to obtain accurate measurements after only one calibration performed prior to a bioreactor cell run.
- The instrument should be small and lightweight.

The instrument includes a quartz cuvette through which the culture medium flows as it is circulated through the bioreactor. The cuvette is sandwiched between light source on one side and a photodetector on the other side. The

light source comprises a red and a green light-emitting diode (LED) that are repeatedly flashed in alternation with a cycle time of 5 s. The responses of the photodiode to the green and red LEDs are processed electronically to obtain a quantity proportional to the ratio between the amounts of green and red light transmitted through the medium.

The medium contains some phenol red, which is an organic pH-indicator dye. Phenol red dissociates to a degree that is a known function of pH and temperature, and its optical absorbance at the wavelength of the green LED (but not at the wavelength of the red LED) varies accordingly. Hence, the pH of the medium can be calculated from the quantity obtained from the photodetector responses, provided that calibration data are available.

During the calibration procedure, the dyed culture medium to be used in the bioreactor is circulated through the cuvette and the photodetector responses are processed and recorded while small amounts of hydrochloric acid are added to the medium from time to time to make the pH decrease in small increments through the pH range from 7.5 to 6.5. For each set of measurements, the

pH is determined by conventional means. Then the resulting data are fitted with a second-order polynomial, the coefficients of which are thereafter used to compute the pH as a function of the aforementioned quantity proportional to the ratio between the amounts of green and red light transmitted.

The cuvette is the only part of the instrument in contact with the culture medium. The cuvette can readily be sterilized, either separately from or as incorporated into the bioreactor system, by use of an autoclave or by use of ethylene oxide. Tests have shown that the error in the pH measurement by this instrument does not range beyond ± 0.1 pH unit, even when a biofilm is present. As required, the instrument is lightweight (total mass, including electronic circuitry, only 150 g) and compact [overall dimensions of 1.0 by 1.5 by 2.5 in. (approximately 2.5 by 3.8 by 6.4 cm)].

*This work was done by Melody M. Anderson and Neal Pellis of Johnson Space Center and Anthony S. Jeevarajan and Thomas D. Taylor of Wyle Laboratories. For further information, contact the Johnson Commercial Technology Office at (281) 483-3809.
MSC-23107*

Imaging of γ -Irradiated Regions of a Crystal

Electron-trapping and photorefractive effects are exploited.

NASA's Jet Propulsion Laboratory, Pasadena, California

A holographic technique has been devised for generating a visible display of the effect of exposure of a photorefractive crystal to γ rays. The technique exploits the space charge that results from

trapping of electrons in defects induced by γ rays.

The technique involves a three-stage process. In the first stage, one writes a holographic pattern in the crystal by use

of the apparatus shown in Figure 1. A laser beam of 532-nm wavelength is collimated and split into signal and reference beams by use of a polarizing beam splitter. On its way to the crystal, the ref-

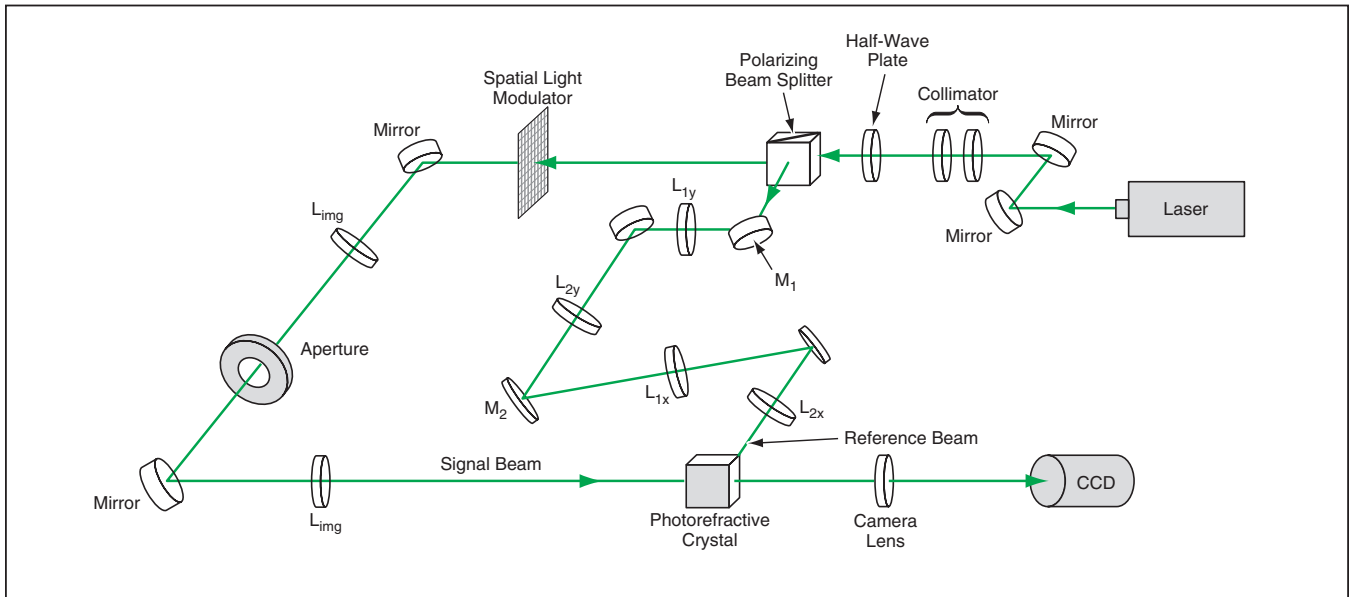


Figure 1. A Hologram Is Formed in a Crystal to be exposed to γ rays. After exposure to γ rays, the crystal is remounted in this apparatus for reading of the hologram.

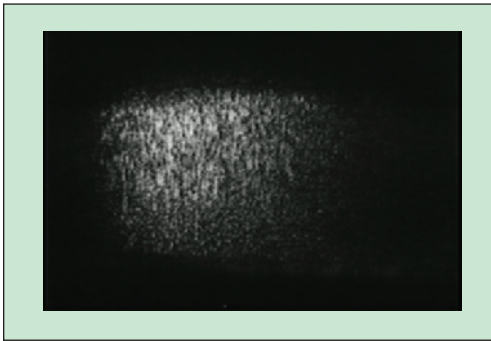


Figure 2. This Image Shows the Effect of γ Rays that have passed through a crystal of Fe:LiNbO₃.

reference beam goes through a two-dimensional optical scanner that contains two pairs of lenses (L_{1y}, L_{2y} and L_{1x}, L_{2x}) and mirrors M_1 and M_2 , which can be rotated by use of micrometer drives to make fine adjustments. The signal beam

is sent through a spatial light modulator that imposes the holographic pattern, then through two imaging lenses L_{img} on its way to the crystal. An aperture is placed at the common focus of lenses L_{img} to suppress high-order diffraction from the spatial light modulator. The hologram is formed by interference between the signal and reference beams.

A camera lens focuses an image of the interior of the crystal onto a charge-coupled device (CCD). If the crystal is illuminated by only the reference beam once the hologram has been formed, then an image of the hologram is formed on the CCD: this phenomenon is exploited to make visible the pattern of γ irradiation of the crystal, as described next.

In the second stage of the process, the crystal is removed from the holographic apparatus and irradiated with γ rays at a dose of about 100 krad. In the third stage of the process, the crystal is remounted in the holographic apparatus in the same position as in the first stage and illuminated with only the reference beam to obtain the image of the hologram as modified by the effect of the γ rays. The orientations of M_1 and M_2 can be adjusted slightly, if necessary, to maximize the intensity of the image. Figure 2 shows such an image that was formed in a crystal of Fe:LiNbO₃.

This work was done by Danut Dragoi, Steven McClure, Allan Johnston, and Tien-Hsin Chao of Caltech for NASA's Jet Propulsion Laboratory. Further information is contained in a TSP (see page 1). NPO-30622

Photodiode-Based, Passive Ultraviolet Dosimeters

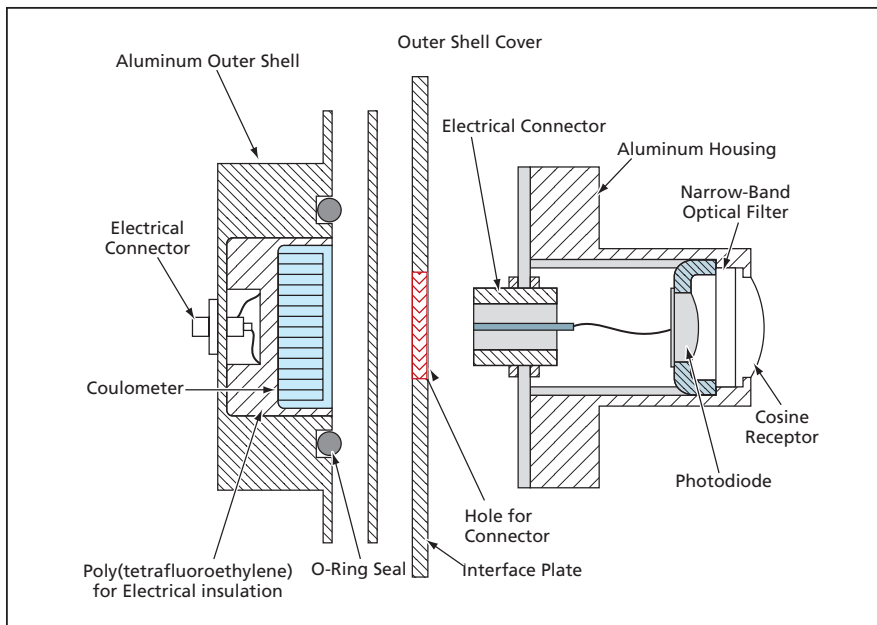
Outputs of photodiodes are fed to coulometers.

Marshall Space Flight Center, Alabama

Simple, passive instruments have been developed for measuring the exposure of material specimens to vacuum ultraviolet (VUV) radiation from the Sun. Each instrument contains a silicon photodiode and a coulometer. The photocharge generated in the photodiode is stored in the coulometer. The accumulated electric charge measured by use of the coulometer is assumed to be propor-

tional to the cumulative dose of VUV radiation expressed in such convenient units as equivalent Sun hours (ESH) [defined as the number of hours of exposure to sunlight at normal incidence]. Intended originally for use aboard spacecraft, these instruments could also be adapted to such terrestrial uses as monitoring the curing of ultraviolet-curable epoxies.

Each instrument includes a photodiode and a coulometer assembly mounted on an interface plate (see figure). The photodiode assembly includes an aluminum housing that holds the photodiode, a poly(tetrafluoroethylene) cosine receptor, and a narrow-band optical filter. The cosine receptor ensures that the angular response of the instrument approxi-



This Simple, Passive Instrument measures the dosage of ultraviolet light in the pass wavelength band of its filter.

mates the ideal angular response (proportional to the cosine of the angle of incidence). The filter is chosen to pass the ultraviolet wavelength of interest in a specific experiment.

The photodiode is electrically connected to the coulometer. The factor of proportionality between the charge stored in the coulometer and ultraviolet dosage (in units of ESH) is established, prior to use, in calibration experiments that involve the use of lamps and current sources traceable to the National Institute of Standards and Technology.

This work was done by Jason A. Vaughn of Marshall Space Flight Center and Perry Gray of Micro Craft, Inc.

This invention is owned by NASA, and a patent application has been filed. For further information, contact Sammy Nabors, MSFC Commercialization Assistance Lead, at (256) 544-5226 or sammy.a.nabors@nasa.gov. Refer to MFS-31316-1.

Discrete Wavelength-Locked External Cavity Laser

The laser is locked internally to frequencies of communication channels.

John H. Glenn Research Center, Cleveland, Ohio

A prototype improved external cavity laser (ECL) was demonstrated in the second phase of a continuing effort to develop wavelength-agile lasers for fiber-optic communications and trace-gas-sensing applications. This laser is designed to offer next-generation performance for incorporation into fiber-optic networks. By eliminating several optical components and simplifying others used in prior designs, the design of this laser reduces costs, mak-

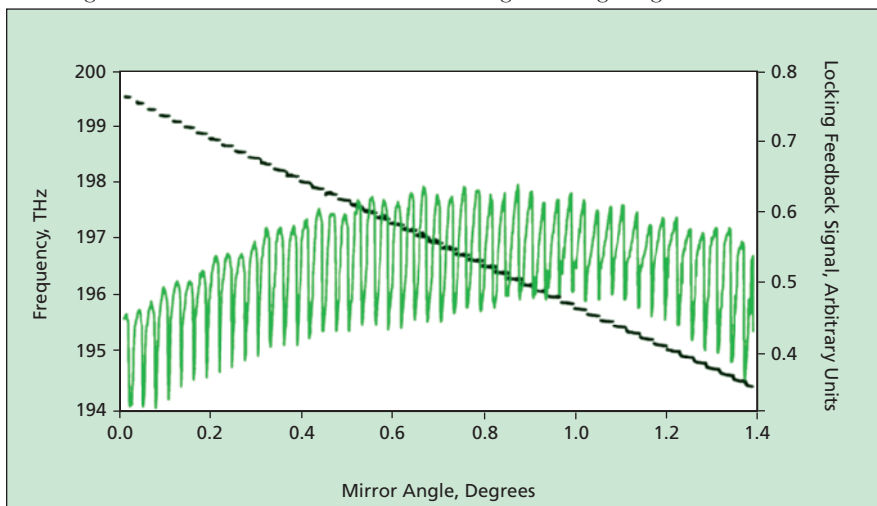
ing lasers of this type very competitive in a price-sensitive market.

Diode lasers have become enabling devices for fiber optic networks because of their cost, compactness, and spectral properties. ECLs built around diode laser gain elements further enhance capabilities by virtue of their excellent spectral properties with significantly increased (relative to prior lasers) wavelength tuning ranges. It is essential to ex-

plot the increased spectral coverage of ECLs while simultaneously insuring that they operate only at precisely defined communication channels (wavelengths). Heretofore, this requirement has typically been satisfied through incorporation of add-in optical components that "lock" the ECL output wavelengths to these specific channels. Such add-in components contribute substantially to the costs of ECL lasers to be used as sources for optical communication networks. Furthermore, the optical alignment of these components, needed to attain the required wavelength precision, is a non-trivial task and can contribute substantially to production costs.

The design of the present improved ECL differs significantly from the designs of prior ECLs. The present design relies on inherent features of components already included within an ECL, with slight modifications so that these components perform their normal functions while simultaneously effecting locking to the required discrete wavelengths. Hence, add-in optical components and the associated cost of alignment can be eliminated.

The figure shows the locking feedback signal, and the frequency locking



The Frequency Varies in Steps as a function of the mirror angle. Each step represents locking to the indicated frequency.

achieved by use of this signal, as a mirror is tilted through a range of angles to tune the ECL through 48 channels. The data for the frequency plot were obtained, simultaneously with the data for the locking-signal plot, by using a scanning Michelson interferometer to precisely determine the ECL wavelength (and, hence, frequency). Given the ability of the Michelson interferometer to obtain highly precise readings, the frequency plot can be taken to be a reliable indication of single-mode operation. The discontinuities in the frequency plot signify the switching of the ECL between channels; in other words, they indicate tuning with locking to discrete frequencies. The peaks of the feedback-locking signal correspond to the cen-

ters, or near centers, of the mirror angle scan through the corresponding channels. Thus, it is clear that when the feedback-locking signal is at a local maximum, the ECL is operating at single frequency at or near the middle frequency of the selected channel. This is all that is required for precisely locking the ECL output wavelength. The locking is achieved without additional external optical components.

Another aspect of the design of this ECL is a provision for the incorporation of a particularly simple microelectromechanical system (MEMS) mirror for wavelength tuning. The simplified motion of the mirror enables facile alignment and rapid tuning, both important in a network source

laser. This ECL is capable of switching wavelengths across the entire frequency band indicated in the figure in a time of less than one millisecond. Other performance characteristics, like the side-mode-suppression ratio and relative-intensity noise, are equal to or better than those of other lasers now available.

This work was done by Jeffrey S. Pilgrim and Joel A. Silver of Southwest Sciences, Inc. for Glenn Research Center.

Inquiries concerning rights for the commercial use of this invention should be addressed to NASA Glenn Research Center, Commercial Technology Office, Attn: Steve Fedor, Mail Stop 4-8, 21000 Brookpark Road, Cleveland, Ohio 44135. Refer to LEW-17313-1.



Flexible Shields for Protecting Spacecraft Against Debris

A report presents the concept of Flexshield — a class of versatile, lightweight, flexible shields for protecting spacecraft against impacts by small meteors and orbiting debris. The Flexshield concept incorporates elements of, but goes beyond, prior spacecraft-shielding concepts, including those of Whipple shields and, more recently, multi-shock shields and multi-shock blankets. A shield of the Flexshield type includes multiple outer layers (called “bumpers” in the art) made, variously, of advanced ceramic and/or polymeric fibers spaced apart from each other by a lightweight foam. As in prior such shields, the bumpers serve to shock an impinging hypervelocity particle, causing it to disintegrate, vaporize, and spread out over a larger area so that it can be stopped by an innermost layer (back sheet). The flexibility of the fabric layers and compressibility of the foam make it possible to compress and fold the shield for transport, then deploy the shield for use. The shield can be attached to a spacecraft by use of snaps, hook-and-pile patches, or other devices. The shield can also contain multilayer insulation material, so that it provides some thermal protection in addition to mechanical protection.

This work was done by Eric L. Christiansen and Jeanne Lee Crews of Johnson Space Center.

This invention is owned by NASA, and a patent application has been filed. Inquiries concerning nonexclusive or exclusive license for its commercial development should be addressed to the Patent Counsel, Johnson Space Center; (281) 483-0837. Refer to MSC-23314.

Part 2 of a Computational Study of a Drop-Laden Mixing Layer

This second of three reports on a computational study of a mixing layer laden with evaporating liquid drops presents the evaluation of Large Eddy Simulation (LES) models. The LES models were evaluated on an existing database that had been generated using Direct Numerical Simulation (DNS). The DNS method and the database are described in the first report of

this series, “Part 1 of a Computational Study of a Drop-Laden Mixing Layer” (NPO-30719), *NASA Tech Briefs*, Vol. 28, No.7 (July 2004), page 59. The LES equations, which are derived by applying a spatial filter to the DNS set, govern the evolution of the larger scales of the flow and can therefore be solved on a coarser grid. Consistent with the reduction in grid points, the DNS drops would be represented by fewer drops, called “computational drops” in the LES context. The LES equations contain terms that cannot be directly computed on the coarser grid and that must instead be modeled. Two types of models are necessary: (1) those for the filtered source terms representing the effects of drops on the filtered flow field and (2) those for the sub-grid scale (SGS) fluxes arising from filtering the convective terms in the DNS equations. All of the filtered-source-term models that were developed were found to overestimate the filtered source terms. For modeling the SGS fluxes, constant-coefficient Smagorinsky, gradient, and scale-similarity models were assessed and calibrated on the DNS database. The Smagorinsky model correlated poorly with the SGS fluxes, whereas the gradient and scale-similarity models were well correlated with the SGS quantities that they represented.

This work was done by Nora Okong'o and Josette Bellan of Caltech for NASA's Jet Propulsion Laboratory. Further information is contained in a TSP (see page 1). NPO-30732

Controllable Curved Mirrors Made From Single-Layer EAP Films

A document proposes that lightweight, deployable, large-aperture, controllable curved mirrors made of reflectively coated thin electroactive-polymer (EAP) films be developed for use in spaceborne microwave and optical systems. In these mirrors, the EAP films would serve as both structures and actuators. EAPs that are potentially suitable for such use include piezoelectric, electrostrictive, ferroelectric, and dielectric polymers. These materials exhibit strains proportional to the squares of applied electric fields. Utilizing this phenomenon, a curved mirror according to the proposal could be made from

a flat film, upon which a nonuniform electrostatic potential (decreasing from the center toward the edge) would be imposed to obtain a required curvature. The effect would be analogous to that of an old-fashioned metalworking practice in which a flat metal sheet is made into a bowl by hammering it repeatedly, the frequency of hammer blows decreasing with distance from the center. In operation, the nonuniform electrostatic potential could be imposed by use of an electron gun. Calculations have shown that by use of a single-layer film made of a currently available EAP, it would be possible to control the focal length of a 2-m-diameter mirror from infinity to 1.25 m.

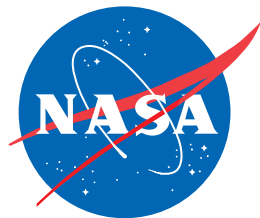
This work was done by Xiaqi Bao, Yoseph Bar-Cohen, and Stewart Sherrit of Caltech for NASA's Jet Propulsion Laboratory. Further information is contained in a TSP (see page 1).

NPO-40275

Demonstration of a Pyrotechnic Bolt-Retractor System

A paper describes a demonstration of the X-38 bolt-retractor system (BRS) on a spacecraft-simulating apparatus, called the Large Mobility Base, in NASA's Flight Robotics Laboratory (FRL). The BRS design was proven safe by testing in NASA's Pyrotechnic Shock Facility (PSF) before being demonstrated in the FRL. The paper describes the BRS, FRL, PSF, and interface hardware. Information on the bolt-retraction time and spacecraft-simulator acceleration, and an analysis of forces, are presented. The purpose of the demonstration was to show the capability of the FRL for testing of the use of pyrotechnics to separate stages of a spacecraft. Although a formal test was not performed because of schedule and budget constraints, the data in the report show that the BRS is a successful design concept and the FRL is suitable for future separation tests.

This work was done by Nick Johnston, Rafiq Ahmed, Craig Garrison, Joseph Gaines, and Jason Waggoner of Marshall Space Flight Center. To obtain a copy of the paper, "X-38 Bolt Retractor Subsystem Separation Demonstration," NASA/TM-2002-212047, September 2002, access <http://trs.nis.nasa.gov/archive/00000604>. MFS-31874



National Aeronautics and
Space Administration